8090–8104 *Nucleic Acids Research, 2018, Vol. 46, No. 16* *Published online 11 August 2018*
doi: 10.1093/nar/gky703

Structural basis for the synergy of 4′- and 2′-modifications on siRNA nuclease resistance, thermal stability and RNAi activity

Joel M. Harp[1], Dale C. Guenther[2], Anna Bisbe[2], Lydia Perkins[2], Shigeo Matsuda[2], Gopal R. Bommineni[2], Ivan Zlatev[2], Donald J. Foster[2], Nate Taneja[2], Klaus Charisse[2], Martin A. Maier[2], Kallanthottathil G. Rajeev[2], Muthiah Manoharan[2,*] and Martin Egli[1,*]

[1]Department of Biochemistry, Vanderbilt University, School of Medicine, Nashville, TN 37232, USA and [2]Alnylam Pharmaceuticals, 300 Third Street, Cambridge, MA 02142, USA

Received May 30, 2018; Editorial Decision July 14, 2018; Accepted July 23, 2018

ABSTRACT

Chemical modification is a prerequisite of oligonucleotide therapeutics for improved metabolic stability, uptake and activity, irrespective of their mode of action, i.e. antisense, RNAi or aptamer. Phosphate moiety and ribose C2′/O2′ atoms are the most common sites for modification. Compared to 2′-*O*-substituents, ribose 4′-*C*-substituents lie in proximity of both the 3′- and 5′-adjacent phosphates. To investigate potentially beneficial effects on nuclease resistance we combined 2′-F and 2′-*O*Me with 4′-*C*α- and 4′-*C*β-OMe, and 2′-F with 4′-*C*α-methyl modification. The α- and β-epimers of 4′-*C*-OMe-uridine and the α-epimer of 4′-*C*-Me-uridine monomers were synthesized and incorporated into siRNAs. The 4′α-epimers affect thermal stability only minimally and show increased nuclease stability irrespective of the 2′-substituent (H, F, OMe). The 4′β-epimers are strongly destabilizing, but afford complete resistance against an exonuclease with the phosphate or phosphorothioate backbones. Crystal structures of RNA octamers containing 2′-F,4′-*C*α-OMe-U, 2′-F,4′-*C*β-OMe-U, 2′-*O*Me,4′-*C*α-OMe-U, 2′-*O*Me,4′-*C*β-OMe-U or 2′-F,4′-*C*α-Me-U help rationalize these observations and point to steric and electrostatic origins of the unprecedented nuclease resistance seen with the chain-inverted 4′β-U epimer. We used structural models of human Argonaute 2 in complex with guide siRNA featuring 2′-F,4′-*C*α-OMe-U or 2′-F,4′-*C*β-OMe-U at various sites in the seed region to interpret in vitro activities of siRNAs with the corresponding 2′-/4′-*C*-modifications.

INTRODUCTION

Ribose 2′-modification is a staple of nucleic acid therapeutics and figures prominently in drugs approved by the US FDA such as Macugen (Pegaptanib), an extensively 2′-F/OMe-modified 28mer anti-VEGF RNA aptamer for treatment of wet age-related macular degeneration (1–3), Mipomersen (Kynamro), a 20mer antisense gapmer with 2′-*O*-(2-methoxyethyl)- (2′-MOE) modified wings against homozygous familial hypercholesterolemia (4,5), and Nusinersen (Spinraza), another MOE-RNA 18mer that mediates alternative splicing for the treatment of spinal muscular atrophy (6). Patisiran, an investigative siRNA-based drug for treatment of hereditary transthyretin-mediated ATTR amyloidosis, currently under FDA review, contains the first generation 2′-*O*-methyl (2′-*O*Me) modification (https://www.drugs.com/history/patisiran.html) (7). In addition to these common modifications, the development of the GalNAc–siRNA conjugate delivery platform has become a transformative approach for developing nucleic acid therapeutic for gene-related diseases emanating from liver (8–14). The success of the GalNAc–siRNA conjugate therapeutic modality vastly relies on ingenious placement of chemical modifications and motifs to the double-stranded siRNA constructs. The recent clinical data substantiate the wide scope of this approach and its immense potential in developing various nucleic acid-based therapeutics (1,7).

Compared to the successful ribose 2′-position modifications mentioned above, modifications at the C4′ and C5′ positions of ribose have been explored in less detail. Recently we examined a series of chirally pure (*R*)- and (*S*)-5′-*C*-methyl pyrimidine modifications and found that they affect thermodynamic stability negatively and in a manner that depends on the configuration at C5′ (15). In regard to protection against nucleases, the (*S*)-epimers with

*To whom correspondence should be addressed. Tel: +1 615 343 8070; Fax: +1 615 343 0704; Email: martin.egli@vanderbilt.edu
Correspondence may also be addressed to Muthiah Manoharan. Tel: +1 617 551 8319; Fax: +1 617 551 8101; Email: mmanoharan@alnylam.com

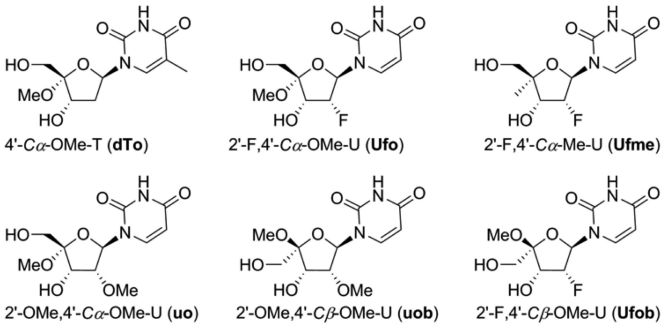

Figure 1. Combined 2′-/4′-*C*-modified uridines and 4′-*C*-modified 2′-deoxythymidine explored in the present contribution.

various 2′-substituents were more effective than the corresponding (*R*)-epimers. Motivated by these findings and given the importance of metabolic stability in the development of oligonucleotide (ON) therapeutics, we embarked on an investigation of the effect of 4′-*C*-modification on the stability of siRNAs (16). We found that similar to 5′-*C*-methyl moieties (15), 4′-*C*-methoxy substituents pose a challenge to nucleases in that they insert themselves between phosphates and in close vicinity of two conserved metal ions (typically Mg^{2+}) at the active site.

Earlier reports of 4′-*C*-modified nucleotides, including 4′-*C*-OMe-2′-deoxynucleotides (17,18) and 2′-F,4′-*C*-F pyrimidine nucleotides (19–21) and their incorporation into oligonucleotides support the notion of a preference for a *Northern* sugar pucker. The thermodynamic stability of RNA duplexes containing such nucleotides is similar to that of the native counterparts (21). Indeed, we found that incorporation of 2′-F,4′-*Cα*-OMe-U (**Ufo**, Figure 1) caused only minor changes to the melting temperature (T_m) of RNA duplexes, whereby the modified ribose adopted a *North* (*N*) C3′-*endo* conformation in the crystal structure of a modified octamer (16). Conversely, insertion of the *β* epimer of 2′-F,4′-*C*-OMe-U (**Ufob**, Figure 1) with an inverted stereocenter at C4′ strongly destabilized an RNA duplex (16).

Here, we report the syntheses of three novel C4′-modified nucleotide (**uo**, **uob** and **Ufme**) building blocks (Figure 1), their incorporation into oligonucleotides and the resulting consequences of these modifications for oligonucleotide thermal stability and nuclease resistance. Crystal structures of self-complementary RNA octamers 5′-r(CGAA**X**UCG)-3′ (**X** = **uo**, **uob**, **Ufme**, **Ufo** (16) and **Ufob**) at high resolution allow insights into the conformational preferences of nucleotides with 2′-,4′-*C*-disubstituted ribose moieties with either *α* or *β* stereochemistry at the C4′-position. The structural data allow a rationalization of the observed thermodynamic and nuclease stability data and point to steric (hydrophobic 4′-*Cα*/*β* substituent) and electrostatic origins (phosphate-phosphate spacing) of the increased protection against nuclease degradation. We extracted 2′-F,4′-*Cα*/*β*-OMe-uridines from modified duplex structures and incorporated them into the seed region of guide siRNA from the crystal structure of the complex with human Argonaute 2 (Ago2), followed by energy minimization using molecular mechanics approaches. These computer models provide a better understanding of the outcomes of in vitro RNAi activity assays that involve mouse hepatocytes and siRNAs modified with 2′-F,4′-*Cα*/*β*-OMe-Us at various sites against mouse transthyretin (*Ttr*).

MATERIALS AND METHODS

Syntheses of RNA oligonucleotides

For general methods/materials and solid phase syntheses of oligonucleotides, see (15,16).

Synthesis of 4′-*C*-methoxy-2′-*O*-methyluridine building blocks

Compound 2. To a solution of compound **1** (20.00 g, 53.70 mmol) (22) in anhydrous THF (280 ml) were added PPh_3 (16.8 g, 64.1 mmol), imidazole (7.60 g, 111.60 mmol), and I_2 (16.40 g, 64.60 mmol) at 0°C. The reaction mixture was stirred at room temperature for 19 h. Additional PPh_3 (4.23 g, 16.10 mmol), imidazole (1.83 g, 26.90 mmol) and I_2 (4.09 g, 16.10 mmol) were added and the mixture was allowed to stir for 1 h. The reaction was quenched by 10% aqueous sodium thiosulfate solution (30 ml). After removing the solvent and volatiles under reduced pressure, the residue was extracted into EtOAc and washed with saturated aqueous $NaHCO_3$ solution. The organic layer was separated, dried over anhydrous Na_2SO_4, filtered and concentrated. The crude material was purified by flash column chromatography on silica gel (eluent: 0–50% EtOAc in hexanes) to obtain compound **2** (25.90 g, 53.70 mmol, 91%, $R_f = 0.54$; developed with 50% EtOAc in hexanes). ^{1}H NMR (400 MHz, DMSO-d_6): δ 11.46 (s, 1H), 7.72 (d, $J = 8.0$ Hz, 1H), 5.86 (d, $J = 5.6$ Hz, 1H), 5.72–5.70 (m, 1H), 4.25 (dd, $J = 5.0$ Hz, 3.8 Hz, 1H), 4.08 (t, $J = 5.4$ Hz, 1H), 3.86–3.82 (m, 1H), 3.54 (dd, $J = 10.6$ Hz, 6.6 Hz, 1H), 3.38 (dd, $J = 10.6$ Hz, 6.2 Hz, 1H), 3.34 (s, 3H), 0.89 (s, 9H), 0.15 (s, 3H), 0.13 (s, 3H). ^{13}C NMR (126 MHz, DMSO-d_6): δ 162.9, 150.4, 141.0, 102.4, 87.0, 83.3, 80.7, 72.8, 57.6, 17.8, 6.4, -4.6, -4.7. HRMS calc. for $C_{16}H_{28}IN_2O_5Si$ $[M+H]^+$ 483.0812; found: 483.0820 (Scheme 1).

Compound 3. To a solution of compound **2** (1.01 g, 2.09 mmol) in CH_3CN (10 ml) was added DBU (0.62 ml, 4.15 mmol) at 0°C. The reaction mixture was stirred at room temperature overnight. After removing the solvent and volatiles under reduced pressure, the residue was purified by flash column chromatography on silica gel (eluent: 0–50% EtOAc in hexanes) to obtain compound **3** (306 mg, 0.86 mmol, 41%, $R_f = 0.42$; developed with 50% EtOAc in hexanes). ^{1}H NMR (400 MHz, DMSO-d_6): δ 11.51 (s, 1H), 7.63 (d, $J = 8.0$ Hz, 1H), 6.04 (d, $J = 5.2$ Hz, 1H), 5.70 (dd, $J = 8.0$ Hz, 1.6 Hz, 1H), 4.78 (d, $J = 4.8$ Hz, 1H), 4.41 (d, $J = 1.2$ Hz, 1H), 4.22 (d, $J = 2.4$ Hz, 1H), 4.13 (t, $J = 5.2$ Hz, 1H), 3.33 (s, 3H), 0.89 (s, 9H), 0.13 (s, 3H), 0.12 (s, 3H). ^{13}C NMR (126 MHz, DMSO-d_6): δ 162.9, 161.0, 150.5, 140.6, 102.6, 87.7, 85.5, 80.3, 69.4, 57.4, 25.6, 17.9, –4.7, –4.8. HRMS calc. for $C_{16}H_{27}N_2O_5Si$ $[M+H]^+$ 355.1689; found: 355.1687.

Compounds 4/5. To a solution of compound **3** (250 mg, 0.71 mmol) in MeOH (10 ml) was added *m*CPBA (268 mg, 1.56 mmol), and the mixture was stirred at room temperature overnight. After removing the solvent and volatiles under reduced pressure, the residue was extracted into CH_2Cl_2

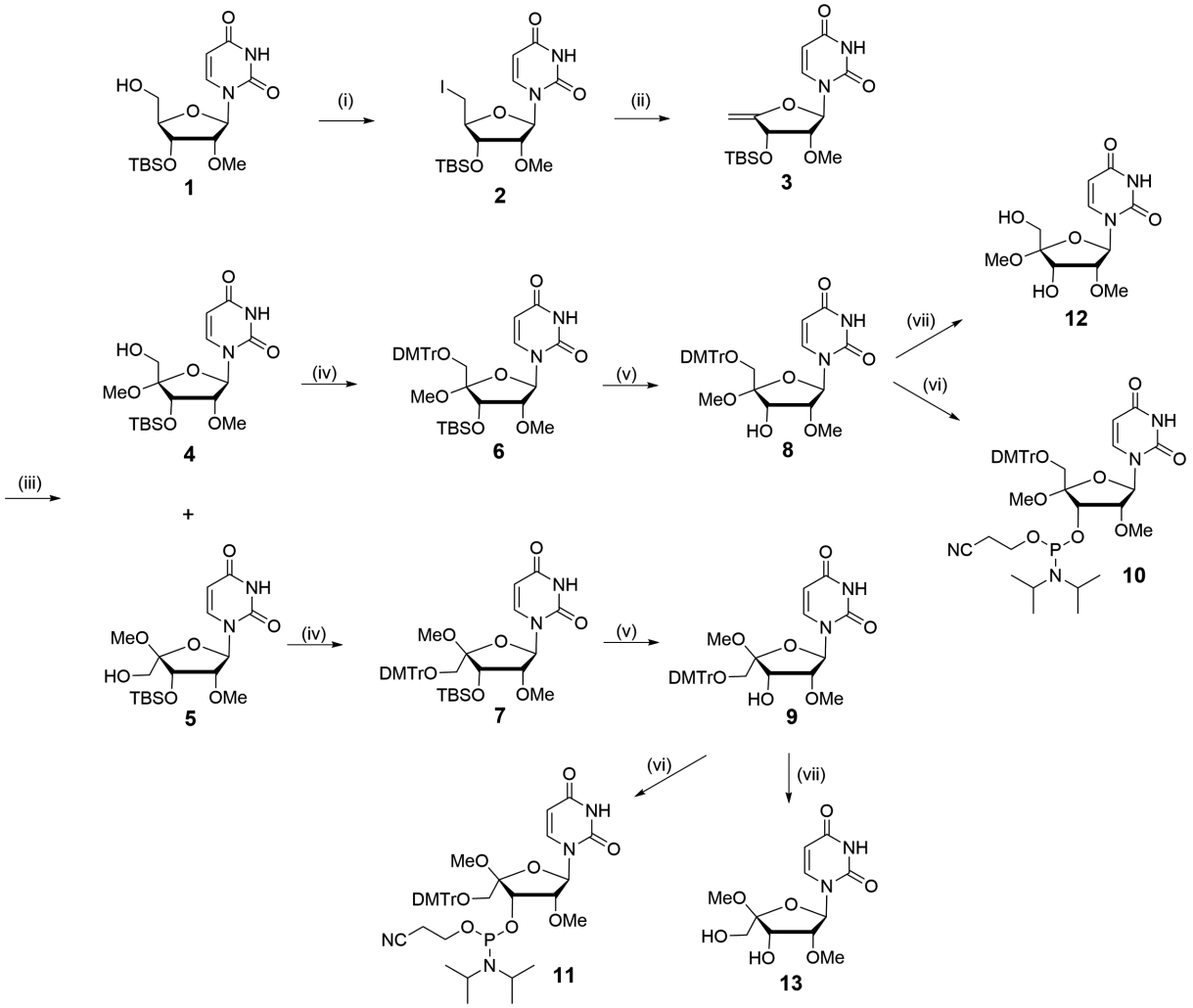

Scheme 1. Reagents and conditions: (i) I_2/PPh_3/imidazole/THF, rt, 20 h, 91%; (ii) DBU/CH_3CN, rt, overnight, 41%; (iii) *m*CPBA/MeOH, rt, overnight, **4**: 67%, **5**: 18%; (iv) DMTrCl/pyridine, rt, overnight, **6**: 83%, **7**: 57%; (v) *n*-TBAF/THF, rt, overnight, **8**: 66%, **9**: 80%; (vi) 2-cyanoethyl *N*,*N*-diisopropylchlorophosphoramidite/DIPEA/CH_2Cl_2, rt, overnight, **10**: 79%, **11**: 64%; (vii) 80% AcOH, rt, overnight, **12**: 96%, **13**: 68%.

and washed with saturated aqueous $NaHCO_3$ solution. The organic layer was separated, dried over anhydrous Na_2SO_4, filtered and concentrated. The crude material was purified by flash column chromatography on silica gel (eluent: 0–5% MeOH in CH_2Cl_2) to obtain compound **4** (114 mg, 0.36 mmol, 40%, $R_f = 0.29$; developed with 5% MeOH in CH_2Cl_2) and compound **5** (52 mg, 0.13 mmol, 18%, $R_f = 0.34$; developed with 5% MeOH in CH_2Cl_2). **Compound 4**: ^{1}H NMR (500 MHz, DMSO-d_6): δ 11.41 (s, 1H), 7.80 (d, $J = 8.0$ Hz, 1H), 5.99 (d, $J = 5.5$ Hz, 1H), 5.70 (d, $J = 8.0$ Hz, 1H), 5.31 (t, $J = 5.5$ Hz, 1H), 4.44 (d, $J = 6.0$ Hz, 1H), 3.89 (t, $J = 6.0$ Hz, 1H), 3.53 (dd, $J = 11.8$ Hz, 5.0 Hz, 1H), 3.42 (dd, $J = 11.8$ Hz, 5.0 Hz, 1H), 3.31 (s, 3H), 3.28 (s, 3H), 0.89 (s, 9H), 0.087 (s, 6H). ^{13}C NMR (126 MHz, DMSO-d_6): δ 162.9, 150.5, 140.4, 106.7, 102.4, 86.3, 81.6, 71.0, 61.4, 58.1, 50.0, 25.7, 18.1, –4.7, –5.0. HRMS calc. for $C_{17}H_{30}N_2NaO_7Si$ $[M+Na]^+$ 425.1720; found: 425.1716. **Compound 5**: ^{1}H NMR (500 MHz, DMSO-d_6): δ 11.45 (s, 1H), 7.50 (d, $J = 8.5$ Hz, 1H), 6.05 (d, $J = 7.5$ Hz, 1H), 5.79 (d, $J = 8.0$ Hz, 1H), 4.76 (t, $J = 5.3$ Hz, 1H), 4.23 (dd, $J = 7.5$ Hz, 4.0 Hz, 1H), 4.17 (d, $J = 4.0$ Hz, 1H), 3.55 (d, $J = 5.0$ Hz, 2H), 3.27 (s, 3H), 3.26 (s, 3H), 0.90 (s, 9H), 0.13 (s, 3H), 0.11 (s, 3H). ^{13}C NMR (126 MHz, DMSO-d_6): δ 162.7, 150.9, 140.1, 110.0, 103.4, 85.4, 82.1, 73.1, 58.1, 55.4, 48.7, 25.8, 18.2, –4.7, –5.1. HRMS calc. for $C_{17}H_{30}N_2NaO_7Si$ $[M+Na]^+$ 425.1720; found: 425.1721.

Compound 6. To a solution of compound **4** (200 mg, 0.50 mmol) in anhydrous pyridine (3 ml) was added DMTrCl (269 mg, 0.80 mmol) at room temperature. The reaction mixture was stirred for 14 h then quenched by the addition of MeOH (0.2 ml). The solvent was removed under reduced pressure, and the residue was extracted with CH_2Cl_2 and saturated $NaHCO_3$ aqueous solution. The organic layer was separated, dried over anhydrous Na_2SO_4, filtered and concentrated. The crude material was purified by flash column chromatography on silica gel (0–50% EtOAc in hexane) to obtain compound **6** (290 mg, 0.41 mmol, 83%, $R_f = 0.39$; developed with 50% EtOAc in hexane). ^{1}H NMR (500 MHz, DMSO-d_6): δ 11.45 (s, 1H), 7.77 (d, $J = 8.0$ Hz, 1H), 7.38–7.31 (m, 4H), 7.27–7.23 (m, 5H), 6.91–6.89 (m, 4H),

5.93 (d, $J = 4.0$ Hz, 1H), 5.36 (d, $J = 8.0$ Hz, 1H), 4.44 (d, $J = 6.5$ Hz, 1H), 3.87 (dd, $J = 6.5$ Hz, 4.0 Hz, 1H), 3.74 (s, 6H), 3.34–3.32 (m, 1H), 3.30 (s, 3H), 3.21 (s, 3H), 3.08 (d, $J = 10.5$ Hz, 1H), 0.79 (s, 9H), 0.019 (s, 3H), -0.041 (s, 3H). ^{13}C NMR (126 MHz, DMSO-d_6): δ 162.90, 158.24, 150.18, 144.18, 141.08, 134.87, 134.77, 129.86, 129.83, 127.87, 127.79, 126.91, 113.22, 113.20, 105.77, 102.01, 88.20, 86.28, 81.05, 71.00, 62.11, 58.15, 55.06, 49.91, 25.61, 17.91, –4.78, –4.98. HRMS calc. for $C_{38}H_{48}N_2NaO_9Si$ $[M+Na]^+$ 727.3027, found 727.3014.

Compound 7. To a solution of compound **5** (200 mg, 0.50 mmol) in anhydrous pyridine (2.5 ml) was added DMTrCl (340 mg, 1.00 mmol) at room temperature. The reaction mixture was stirred for 18 h then quenched by addition of MeOH (0.2 ml). The solvent was removed under reduced pressure, and the residue was extracted into CH_2Cl_2 and washed with saturated aqueous $NaHCO_3$ solution. The organic layer was separated, dried over anhydrous Na_2SO_4, filtered and concentrated. The crude material was purified by flash column chromatography on silica gel (eluent: 0–50% EtOAc in hexane) to obtain compound **7** (200 mg, 0.28 mmol, 57%, $R_f = 0.47$; developed with 50% EtOAc in hexane). ^{1}H NMR (400 MHz, DMSO-d_6): δ 11.51 (s, 1H), 7.67 (d, $J = 8.0$ Hz, 1H), 7.43–7.41 (m, 2H), 7.32–7.22 (m, 7H), 6.90–6.87 (m, 4H), 6.14–6.11 (m, 1H), 5.81 (d, $J = 8.0$ Hz, 1H), 4.21–4.19 (m, 2H), 3.73 (s, 6H), 3.58 (d, $J = 10.8$ Hz, 1H), 3.34–3.33 (m, 1H), 3.32 (s, 3H), 3.28 (s, 3H), 2.96 (d, $J = 10.4$ Hz, 1H), 0.68 (s, 9H), 0.016 (s, 3H), -0.14 (s, 3H). ^{13}C NMR (101 MHz, DMSO-d_6): δ 162.9, 158.1, 150.9, 144.6, 140.3, 135.5, 135.1, 129.8, 129.7, 127.8, 127.7, 126.7, 113.2, 113.1, 108.3, 103.1, 86.3, 85.9, 81.5, 74.2, 63.2, 58.3, 55.0, 51.5, 25.5, 17.7, –4.4, –5.2. HRMS calc. for $C_{38}H_{48}N_2NaO_9Si$ $[M+Na]^+$ 727.3027; found: 727.3015.

Compound 8. Compound **6** (5.46 g, 7.75 mmol) was treated with 1 M *n*-TBAF (11.60 ml, 11.60 mmol) in THF (80 ml) at room temperature overnight. The solvent was removed and the residue was purified by flash column chromatography on silica gel (eluent: 33–80% EtOAc in hexanes) to obtain compound **8** (3.00 g, 5.08 mmol, 66%, $R_f = 0.19$; developed with 50% EtOAc in hexanes). ^{1}H NMR (400 MHz, DMSO-d_6): δ 11.45 (s, 1H), 7.72 (d, $J = 8.0$ Hz, 1H), 7.40–7.38 (m, 2H), 7.34–7.31 (m, 2H), 7.27–7.24 (m, 5H), 6.92–6.89 (m, 4H), 5.85 (d, $J = 2.8$ Hz, 1H), 5.37 (d, $J = 8.0$ Hz, 1H), 4.70 (d, $J = 10.0$ Hz, 1H), 4.50 (dd, $J = 10.4$ Hz, 6.8 Hz, 1H), 3.87 (dd, $J = 7.0$ Hz, 3.0 Hz, 1H), 3.74 (s, 6H), 3.38 (s, 3H), 3.24 (d, $J = 10.0$ Hz, 1H), 3.12 (s, 3H), 3.09 (d, $J = 10.0$ Hz, 1H). ^{13}C NMR (126 MHz, DMSO-d_6): δ 163.0, 158.2, 150.1, 144.5, 141.2, 135.1, 135.0, 129.79, 129.77, 127.9, 127.7, 126.8, 113.3, 105.3, 102.0, 88.7, 86.0, 81.4, 70.9, 61.8, 58.6, 55.0, 49.1. HRMS calc. for $C_{32}H_{34}N_2NaO_9$ $[M+Na]^+$ 613.2162; found: 613.2158.

Compound 9. Compound **7** (2.10 g, 2.98 mmol) was treated with 1 M *n*-TBAF (6.00 ml, 6.00 mmol) in THF (30 ml) at room temperature overnight. The solvent was removed and the residue was purified by flash column chromatography on silica gel (eluent: 33–80% EtOAc in hexanes) to obtain compound **9** (1.40 g, 2.37 mmol, 80%, $R_f = 0.18$; developed with 50% EtOAc in hexanes). ^{1}H NMR (400 MHz, DMSO-d_6): δ 11.41 (s, 1H), 7.48–7.46 (m, 2H), 7.42 (d, $J = 8.0$ Hz, 1H), 7.35–7.29 (m, 6H), 7.25–7.21 (m, 1H), 6.89 (d, $J = 8.8$ Hz, 4H), 6.09 (d, $J = 7.6$ Hz, 1H), 5.79 (d, $J = 6.0$ Hz, 1H), 5.74 (d, $J = 8.0$ Hz, 1H), 4.34 (dd, $J = 6.0$ Hz, 4.0 Hz, 1H), 4.26 (dd, $J = 7.4$ Hz, 4.2 Hz, 1H), 3.74 (s, 3H), 3.73 (s, 3H), 3.48 (d, $J = 9.6$ Hz, 1H), 2.83 (s, 3H), 2.83 (d, $J = 9.6$ Hz, 1H). ^{13}C NMR (101 MHz, DMSO-d_6): δ 162.7, 158.1, 151.0, 144.6, 140.1, 135.4, 134.9, 130.0, 129.8, 127.79, 127.75, 126.7, 113.1, 113.1, 109.9, 103.3, 85.38, 85.36, 82.1, 71.2, 57.3, 57.0, 55.0, 48.2. HRMS calc. for $C_{32}H_{34}N_2NaO_9$ $[M+Na]^+$ 613.2162; found: 613.2170.

Compound 10. To a solution of compound **8** (2.75 g, 4.66 mmol) in anhydrous CH_2Cl_2 (25 ml) and *N,N*-diisopropylethylamine (2.44 ml, 14.00 mmol) was added 2-cyanoethyl *N*,*N*-diisopropylchlorophosphoramidite (1.57 ml, 7.04 mmol). The reaction mixture was stirred at room temperature overnight under argon atmosphere. The reaction mixture was diluted with CH_2Cl_2 (200 ml) then washed with saturated aqueous $NaHCO_3$ solution (100 ml). The organic layer was separated, dried over anhydrous Na_2SO_4, filtered and concentrated. The crude material was purified by flash column chromatography on silica gel (eluent: 33–50% EtOAc in hexane) to obtain compound **10** (2.90 g, 3.67 mmol, 79%, $R_f = 0.25$ developed with 50% EtOAc in hexane) as a white foam. ^{1}H NMR (400 MHz, CD_3CN): δ 9.16 (s, 1H), 7.75–7.64 (m, 1H), 7.46–7.40 (m, 2H), 7.35–7.26 (m, 7H), 6.90–6.86 (m, 4H), 6.02–5.98 (m, 1H), 5.19–5.16 (m, 1H), 4.82–4.68 (m, 1H), 3.95–3.91 (m, 1H), 3.77–3.76 (m, 6H), 3.70–3.59 (m, 4H), 3.47–3.42 (m, 4H), 3.28–3.18 (m, 4H), 2.70–2.47 (m, 2H), 1.19–1.06 (m, 12H). ^{31}P NMR (162 MHz, CD_3CN): δ 150.67, 150.23. ^{13}C NMR (126 MHz, CD_3CN): δ 163.9, 159.7, 159.8, 151.1, 145.6, 141.5, 141.5, 136.2, 136.1, 131.4, 131.3, 129.2, 129.2, 128.9, 128.1, 119.5, 114.1, 107.8, 107.7, 102.9, 90.4, 90.1, 88.1, 83.4, 83.2, 83.1, 72.5, 72.4, 71.7, 71.6, 63.4, 62.7, 59.9, 59.7, 59.6, 59.55, 55.95, 55.93, 50.9, 50.6, 44.15, 44.13, 44.05, 44.03, 25.13, 25.07, 25.03, 25.01, 25.0, 24.9, 24.85, 21.0, 20.9. HRMS calc. for $C_{41}H_{51}N_4NaO_{10}P$ $[M+Na]^+$ 813.3241; found; 813.3242.

Compound 11. To a solution of compound **9** (2.30 g, 3.89 mmol) in anhydrous CH_2Cl_2 (19 ml) and *N,N*-diisopropylethylamine (2.04 ml, 11.70 mmol) was added 2-cyanoethyl *N*,*N*-diisopropylchlorophosphoramidite (1.36 ml, 5.84 mmol). The reaction mixture was stirred at room temperature for 16 h under argon atmosphere. The reaction mixture was diluted with CH_2Cl_2 (200 ml) then washed with saturated aqueous $NaHCO_3$ solution (100 ml). The organic layer was separated, dried over anhydrous Na_2SO_4, filtered and concentrated. The crude material was purified by flash column chromatography on silica gel (eluent: 33–50% EtOAc in hexanes) to obtain **11** (1.98 g, 2.50 mmol, 64%, $R_f = 0.59$, 0.52 developed with 67% EtOAc in hexanes) as a white foam. ^{1}H NMR (500 MHz, CD_3CN): δ 8.93 (s, 1H), 7.55–7.48 (m, 3H), 7.40–7.22 (m, 7H), 6.88–6.86 (m, 4H), 6.12 (dd, $J = 10.5$ Hz, 6.5 Hz, 1H), 5.70 (dd, $J = 8.3$ Hz, 5.3 Hz, 1H), 4.44–4.34 (m, 1H), 4.23–4.15 (m, 1H), 3.77 (s, 6H), 3.63–3.37 (m, 8H), 3.26–3.08 (m, 4H), 2.66 (t, $J = 6.0$ Hz, 1H), 2.42–2.31 (m, 1H), 1.26–0.98 (m, 12H). ^{31}P NMR (202 MHz, CD_3CN): δ 152.90, 150.85. ^{13}C NMR (126 MHz, CD_3CN): δ 163.6, 159.71, 159.69, 151.9, 146.0, 141.2, 136.7, 136.6, 131.31, 131.26, 131.10, 131.0, 129.2, 128.86, 128.76, 127.84, 119.31, 114.05, 113.98, 110.32, 110.29, 104.06, 87.22, 86.89, 83.52, 75.24, 75.15, 61.6, 59.1, 59.0, 58.8, 55.9, 51.23, 44.1, 44.0, 24.9,

24.83, 24.76, 20.9, 20.8. HRMS calc. for $C_{41}H_{51}N_4NaO_{10}P$ $[M+Na]^+$ 813.3241; found: 813.3246.

Compound 12. Compound **8** (190 mg, 0.32 mmol) was treated in 80% AcOH (20 ml) overnight. After removing the solvent, the residue was purified by flash column chromatography on silica gel (eluent: 0–10% MeOH in CH_2Cl_2) to obtain **12** (89 mg, 0.31 mmol, 96%, $R_f = 0.31$ developed with 10% MeOH in CH_2Cl_2) as a white solid. ^{1}H NMR (400 MHz, DMSO-d_6): δ 11.41 (s, 1H), 7.79 (d, $J = 8.0$ Hz, 1H), 5.94 (d, $J = 4.0$ Hz, 1H), 5.67 (d, $J = 8.4$ Hz, 1H), 5.28 (brs, 1H), 4.68 (d, $J = 8.8$ Hz, 1H), 4.27 (dd, $J = 8.8$ Hz, 6.4 Hz, 1H), 3.81 (dd, $J = 6.8$ Hz, 4.0 Hz, 1H), 3.60 (d, J = 11.6 Hz, 1H), 3.45–3.42 (m, 1H), 3.34 (s, 3H), 3.28 (s, 3H). ^{13}C NMR (126 MHz, DMSO-d_6): δ 163.0, 150.3, 140.5, 106.4, 102.2, 87.0, 81.8, 69.5, 60.2, 58.1, 49.5. HRMS calc. for $C_{11}H_{16}N_2NaO_7$ $[M+Na]^+$ 311.0855, found 311.0850.

Compound 13. Compound **9** (150 mg, 0.25 mmol) was treated in 80% AcOH (5 ml) overnight. After removing the solvent, the residue was purified by flash column chromatography on silica gel (eluent: 0–10% MeOH in CH_2Cl_2) to obtain **13** (50 mg, 0.17 mmol, 68%, $R_f = 0.25$ developed with 10% MeOH in CH_2Cl_2) as a white solid. ^{1}H NMR (400 MHz, DMSO-d_6): δ 11.43 (s, 1H), 7.48 (d, $J = 8.4$ Hz, 1H), 6.11 (d, $J = 7.6$ Hz, 1H), 5.79 (dd, $J = 8.0$ Hz, 2.0 Hz, 1H), 5.50 (d, $J = 5.2$ Hz, 1H), 4.76 (t, $J = 5.8$ Hz, 1H), 4.19 (dd, $J = 7.6$ Hz, 4.0 Hz, 1H), 4.05 (t, $J = 4.6$ Hz, 1H), 3.65 (dd, $J = 12.0$ Hz, 5.6 Hz, 1H), 3.50 (dd, $J = 12.0$ Hz, 5.2 Hz, 1H), 3.27 (s, 3H), 3.25 (s, 3H). ^{13}C NMR (101 MHz, Methanol-d_4): δ 165.72, 152.63, 142.19, 111.87, 104.12, 88.22, 84.20, 72.89, 58.36, 57.48. HRMS calc. for $C_{11}H_{16}N_2NaO_7$ $[M+Na]^+$ 311.0855, found 311.0854.

Synthesis of 4′-*Cα*-methyl-2′-fluorouridine building block

Compound 15. To a solution of compound **14** (780 mg, 3.00 mmol) (23) in anhydrous pyridine (30 ml) was added DMTrCl (2.00 g, 5.90 mmol) at room temperature. The reaction mixture was stirred for 48 h, then quenched by addition of MeOH (5 ml). The solvent and volatiles were removed under reduced pressure, and the residue was extracted into CH_2Cl_2 and washed with saturated aqueous $NaHCO_3$ solution. The organic layer was separated, dried over anhydrous Na_2SO_4, filtered and concentrated. The crude material was purified by flash column chromatography on silica gel (eluent: 0–100% EtOAc in hexanes) to obtain compound **15** (1.50 g, 2.67 mmol, 89%). ^{1}H NMR (400 MHz, DMSO-d_6): δ 11.41 (s, 1H), 7.73 (d, $J = 8.0$ Hz, 1H), 7.39–7.36 (m, 2H), 7.31 (t, $J = 7.6$ Hz, 2H), 7.26–7.23 (m, 5H), 6.89 (dd, $J = 9.0$ Hz, 3.0 Hz, 4H), 5.92 (dd, $J = 19.6$ Hz, 1.6 Hz, 1H), 5.70 (d, $J = 6.4$ Hz, 1H), 5.26 (d, $J = 8.0$ Hz, 1H), 5.14 (m, 1H), 4.43 (m, 1H), 3.74 (s, 6H), 3.13 (d, $J = 10.0$ Hz, 1H), 3.03 (d, $J = 10.0$ Hz, 1H), 1.15 (s, 3H). ^{19}F NMR proton coupled spectrum (376 MHz, DMSO-d_6): δ -201.22, -201.27, -201.29, -201.34, -201.37, -201.42, -201.43, -201.48. ^{13}C NMR (126 MHz, DMSO-d_6): δ 163.10, 158.10, 158.08, 150.13, 144.69, 141.19, 135.34, 135.10, 129.80, 129.77, 127.86, 127.72, 126.75, 113.20, 101.37, 95.00, 93.51, 88.14, 87.86, 85.69, 85.46, 69.46, 69.34, 66.72, 55.03, 55.02, 18.17, 18.14. HRMS calc. for $C_{31}H_{31}FN_2NaO_7$ $[M+Na]^+$ 585.2013, found 585.2023 (Scheme 2).

Compound 16. To a solution of compound **15** (1.23 g, 2.19 mmol) in anhydrous CH_2Cl_2 (20 ml) and *N,N*-diisopropylethylamine (1.60 ml, 9.19 mmol) was added 2-cyanoethyl *N,N*-diisopropylchloro-phosphoramidite (1.00 ml, 4.48 mmol). The reaction mixture was stirred at room temperature for overnight under argon atmosphere. The reaction mixture was diluted with CH_2Cl_2 (200 ml) then washed with saturated $NaHCO_3$ aqueous solution (100 ml). The organic layer was separated, dried over anhydrous Na_2SO_4, filtered and concentrated. The crude material was purified by flash column chromatography on silica gel (0–60% EtOAc in hexane) to obtain compound **16** (1.30 g, 1.70 mmol, 78%) as a white foam. ^{1}H NMR (400 MHz, DMSO-d_6): δ 11.42 (s, 1H), 7.81 (d, $J = 8.0$ Hz, 1H), 7.39 (t, $J = 7.4$ Hz, 2H), 7.32–7.22 (m, 7H), 6.90–6.84 (m, 4H), 5.98–5.90 (m, 1H), 5.42–5.23 (m, 2H), 4.81–4.61 (m, 1H), 3.78–3.73 (m, 7H), 3.63–3.49 (m, 3H), 3.16–3.06 (m, 2H), 2.79–2.60 (m, 2H), 1.20–0.94 (m, 15H). ^{31}P NMR (162 MHz, DMSO-d_6): δ 151.01, 150.96, 150.52, 150.47. ^{19}F NMR proton coupled spectrum (376 MHz, CD_3CN) δ -192.92, –192.94, –192.96, –192.98, –193.00, –193.03, –193.05, –193.08, –193.11, –193.12, –193.14, –193.17, –193.19, –193.96, –193.99, –194.01, –194.03, –194.04, –194.06, –194.08, –194.11, –194.13, –194.15, –194.17, –194.18, –194.20, –194.22, –194.25. ^{13}C NMR (126 MHz, DMSO-d_6): δ 163.18, 163.16, 158.13, 158.09, 150.13, 150.09, 144.59, 142.04, 141.79, 135.18, 135.06, 134.99, 129.82, 129.78, 129.76, 127.80, 127.75, 127.69, 126.77, 126.73, 118.93, 118.66, 113.15, 113.13, 101.42, 101.37, 94.35, 93.66, 92.86, 92.16, 89.73, 89.43, 89.15, 85.73, 85.66, 85.29, 85.26, 85.19, 71.25, 70.38, 70.26, 70.15, 66.35, 65.99, 58.71, 58.56, 58.46, 58.32, 55.02, 55.00, 54.97, 54.95, 54.90, 42.79, 42.68, 42.58, 24.40, 24.34, 24.28, 24.22, 24.18, 19.82, 19.76, 18.40, 18.37, 18.10, 18.08. HRMS calc. for $C_{40}H_{49}FN_4O_8P$ $[M+H]^+$ 763.3272, found 763.3265.

All NMR spectra are depicted in the Supplementary Material. Syntheses of oligonucleotides were carried out as described.

Determination of UV thermal melting temperatures

Thermal melting temperatures were measured with equimolar concentrations of both strands (2.5 μM) in 1× PBS ([NaCl] = 137 mM, [KCl] = 2.7 mM, [Na_2HPO_4] = 10 mM, [KH_2PO_4] = 1.8 mM, pH 7.4) by monitoring A_{260} with increasing temperature (1°C/min). Values were reported as the maximum of the first derivative and are the average of at least two experiments (Table 1).

Stability of modified oligonucleotides against 3′-specific exonuclease degradation

The modified oligonucleotides were prepared in a final concentration of 0.1 mg/ml in 50 mM Tris (pH 7.2), 10 mM $MgCl_2$. The exonuclease (150 mU/ml, SVPDE) was added immediately prior to analysis via IEX HPLC (Dionex DNAPac PA200, 4 × 250 mm) using a gradient of 37–52% mobile phase, B in A (1 M NaBr, 20 mM sodium phosphate, pH 11, 15% MeCN; A: 20 mM sodium phosphate, pH 11, 15% MeCN) over 7.5 min with a flow of 1 ml/min. Samples were analyzed at given time points for up to 24

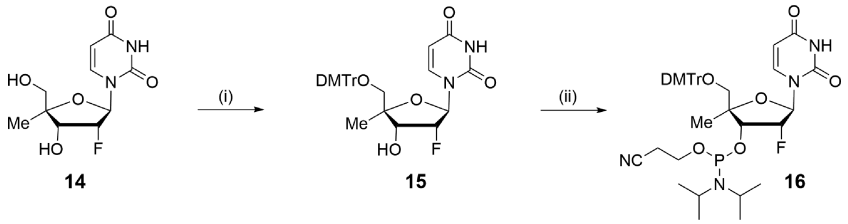

Scheme 2. Reagents and conditions: (i) DMTrCl/pyridine, rt, 48 h, 89% (ii) 2-cyanoethyl *N*,*N*-diisopropylchloro-phosphoramidite, DIPEA/CH_2Cl_2, rt, overnight, 78%.

Table 1. Relative melting temperatures T_m of modified duplexes[a]

			ΔT_m [°C]							
ON	Duplex	X =	**Uf**[b]	**Ufme**	**Ufo**[b]	**Ufob**[b]	**u**	**uo**	**uob**	**dTo**
1	5′-r(UACAG**X**CUAUGU)		+0.7	-0.5	0	-8.9	+0.2	0	-6.3	+2.0
2	3′-r(AUGUCAGAUACA)									
3	5′-d(TACAG**X**CTATGT)		+2.1	-2.0	-1.2	-4.7	+1.5	-1.0	-1.9	+0.9
2	3′-r(AUGUCAGAUACA)									
3	5′-d(TACAG**X**CTATGT)		-1.6	-5.2	-4.2	-8.7	-0.9	-3.9	-4.7	-1.7
4	3′-d(ATGTCAGATACA)									

[a] T_m was measured as the maximum of the first derivative of the melting curve (A_{260} vs T) of pre-hybridized duplexes (2.5 μM) in 1x PBS ([NaCl] = 137 mM, [KCl] = 2.7 mM, [Na_2HPO_4] = 10 mM, [KH_2PO_4] = 1.8 mM, pH 7.4). ΔT_m is calculated with respect to the unmodified duplex: T_m (ON1(**U**):ON2) = 53.2 °C, T_m (ON3(**T**):ON2) = 41.5 °C, T_m (ON3(**T**):ON4) = 42.9 °C. [b] Data from ref. 16.

h. The quantity of full-length oligonucleotide was determined as the area under the curve at A_{260}. Percent full-length oligonucleotide at a given time was calculated with respect to the area under the curve at $t = 0$. The enzyme activity was verified for each experiment by including an oligodeoxythymidylate with a terminal phosphorothioate linkage (5′-dT_{19}•dT). Each aliquot of enzyme was thawed just prior to the experiment. The half-life was determined by fitting to first order kinetics.

RT qPCR for *Ttr* mRNA quantification

Primary mouse hepatocytes (PMH) were cultured in Williams E Medium with 10% fetal bovine serum. Transfection of cells using RNAiMAX reagent was done as per the manufacturer′s recommended protocol. Thus, cells were thawed immediately prior to transfection and then plated onto 384-well plates with a seed density of ∼5000 cells/well. Pre-incubated lipid/siRNA complex (0.1 μl RNAiMax, siRNA, in 5 μl Opti-MEM for 15 min) was added to a 384-well collagen-coated plate (BioCoat; Corning) and cells were incubated for 20 h at 37°C in an atmosphere of 5% CO_2. We used eight 6-fold serial dilutions ranging from 10 to 0.036 nM to perform dose response experiments. Media was removed before washing and lysing the cells. Using Dynabeads mRNA isolation kit according to manufacturer′s protocol, RNA was extracted and subsequently reverse-transcribed with the ABI high capacity cDNA reverse transcription kit. Quantification was done by real-time PCR, whereby the cDNA (2 μl) was added to a master mix that contained 0.5 μl mouse *Gapdh* TaqMan Probe, 0.5 μl *Ttr* TaqMan probes, and 5 μl Lightcycler 480 probe master mix per well in a 384-well 50 plate. Real-time PCR was accomplished in an ABI 7900HT RT-PCR system using the ΔΔCt (RQ) assay. Each duplex and concentration was tested in four biological replicates.

Crystallization experiments

Crystals of **Ufme**, the RNA 8-mer oligonucleotide containing 4′-*Cα*-Me,2′-F U, were grown by the sitting-drop vapor diffusion technique. Crystals were obtained from drops (0.6 μl) containing oligonucleotide (0.5 mM), sodium cacodylate (20 mM, pH 6.5), magnesium chloride (10 mM), cobalt(III) hexamine chloride (10 mM), 2-methyl-2,4-pentanediol, and MPD (20%), equilibrated against a reservoir containing 70 μl of sodium cacodylate (40 mM, pH 6.5), magnesium chloride (20 mM), cobalt(III) hexamine chloride (20 mM), and MPD (40%).

Crystals of **uob**, the RNA 8-mer oligonucleotide containing 4′-*Cβ*-OMe,2′-*O*Me U, were grown by the hanging-drop vapor diffusion technique. Crystals were obtained from drops (5.0 μl) containing oligonucleotide (0.5 mM), sodium cacodylate (20 mM, pH 6.6), sodium chloride (40 mM), potassium chloride (6 mM), magnesium chloride (10 mM), and spermine tetrahydrochloride (6 mM) that were equilibrated against a reservoir of MPD (0.9 ml, 35–50%).

Crystals of **uo**, the RNA 8-mer oligonucleotide containing 4′-*Cα*-OMe,2′-*O*Me U, were grown by the sitting-drop vapor diffusion technique. Crystals were obtained from drops (0.8 μl) containing oligonucleotide (0.5 mM), sodium cacodylate (20 mM, pH 6.0), potassium chloride (40 mM), magnesium chloride (10 mM), spermine tetrahydrochloride (6 mM), and MPD (5%), equilibrated against a reservoir containing MPD (70 μl, 40%).

Crystals of **Ufob**, the RNA 8-mer oligonucleotide containing 4′-*Cβ*-OMe,2′-F U, were grown by the hanging-drop vapor diffusion technique. Crystals were obtained from drops (4.0 μl) containing oligonucleotide (0.25 mM), ammonium sulfate (1.875 M), magnesium chloride (7.5 mM), and MES (pH 5.6, 75 mM), equilibrated against a reservoir containing 0.9 ml of ammonium sulfate (2.5 M), magnesium chloride (10 mM), and MES (pH 5.6, 100 mM).

X-ray diffraction data collection, processing, structure solution and refinement

All crystals of modified self-complementary RNA octamers were mounted without further cryo-protection and flash-cooled in liquid nitrogen. Diffraction data were collected on the 21-ID-D beam line of the Life Sciences Collaborative Access Team (LS-CAT) at the Advanced Photon Source

(APS), located at Argonne National Laboratory (Argonne, IL). Crystals were maintained at 100 K during data collection using a Dectris Eiger 9M hybrid photon counting detector. Data were collected using X-ray energy of 13 500 eV for Br-SAD phasing. Diffraction data were indexed, scaled, and merged using the expert system, xia2 (24), and DIALS (25). Selected crystal data and data collection parameters are summarized in Table 2.

SAD data were phased using SHELXC, SHELXD and SHELXE (26–28) through HKL2MAP (29). The resulting maps were used to manually build the model using COOT (30). The modified residues were built into the electron density and refinement continued with a dictionary created using PRODRG (31). Molecular replacement phasing for **Ufme** was done using the **Ufo** structure, PDB code 5VR4, as search model. Molecular replacement and all refinement was done using the PHENIX package (32). Refinement parameters are summarized in Table 2.

Molecular modeling

Coordinates of the complexes between miR-20A and human Ago2 (33) were retrieved from the Protein Data Bank (PDB ID 4F3T). Coordinates for 2′-F,4′-*Cα*-OMe-U (**Ufo**) and 2′-F,4′-*Cβ*-OMe-U (**Ufob**) nucleotides were taken from the structures of octamers containing the corresponding modifications (residue 5.A) along with the 5′- and 3′-phosphate groups. The match option in UCSF Chimera (34) was used to overlay modified nucleotides with either A at position 2 of the RNA strand (4′-*Cα*- and 4′-*Cβ*-epimers), A at position 4 (4′-*Cα*-epimer), or U at position 6 (4′-*Cβ*-epimer). In the case of the *β*-epimer, the superimposition initially was limited to the two phosphate groups, followed by rotation around the axis between them to identify an orientation of the modified nucleoside that would result in as few steric conflicts as possible. The only torsion angles that were adjusted to allow an optimal fit with the rest of the backbone concerned *ζ* (5′-phosphate) and *α* (3′-phosphate). Models of complexes with modified RNA strands built in this fashion were subsequently refined in UCSF Chimera using the Amber ff12SB force field in combination with Gasteiger potentials and steepest descent as well as conjugate gradient minimization until convergence.

RESULTS

Syntheses and conformations of 4′-*Cα*- and 4′-*Cβ*-epimeric building blocks

The **Ufo** and **Ufob** (16) and **dTo** (35) phosphoramidite building blocks were synthesized as reported, and the synthetic procedures for **Ufme**, **uo** and **uob** are described in the Methods section. All modified oligonucleotides were synthesized *via* standard solid phase phosphoramidite chemistry and products were characterized with mass spectrometry (Supplementary Table S1). The sugar conformations preferred by 4′-*C*-modified nucleosides were estimated based on ^{1}H NMR $^{3}J_{H1'\text{-}H2'}$ coupling constants (Table 3). Like **dTo** and 2′-deoxy-2′-fluoro-U (**Uf**), the 4′-*Cα*-OMe and -Me epimers (**Ufo**, **Ufme**, **uo**) have a high tendency of adopting an *N*-type (C3′-*endo*) pucker. Conversely, the *N*-type pucker is clearly less favored by *Cβ*-epimers (**Ufob**, **Uob**) at the nucleoside levels.

Thermal stability

Thermal melting temperatures (T_m) were measured for RNA, DNA, or DNA:RNA duplexes containing a single, centrally located modified nucleotide (Table 1). Modification at the 2′-position of uridine (i.e., 2′-F or 2′-*O*Me; **Uf** or **u** respectively) leads to increased thermal stability in the context of RNA or DNA:RNA duplexes (up to +2.1°C), but is slightly destabilizing in DNA duplexes (ΔT_m = -1.6 or -0.9°C). In general, addition of a 4′-*Cα*-substituent to 2′-modified nucleotides (i.e., **Ufme**, **Ufo**, **uo**) is well tolerated within an RNA duplex with similar T_m-values as unmodified RNA. This could be due to favorable RNA-like C3′-*endo* conformational pre-organization of the monomers, which is compensated for by destabilizing effects such as an altered charge distribution on the furanose ring or solvation of the duplex (16). Notably, the crystal structure of **Ufo** revealed that the methyl group of 4′-*Cα*-OMe, is positioned roughly equidistantly from the 5′- and 3′-phosphate groups and likely does not exert a significant steric distortion (16). In the context of DNA:RNA (ON3(X):ON2)) or DNA:DNA (ON3(X):ON4) duplexes, thermal destabilization is apparent. Regardless of the 2′-substituent, incorporation of 4′-*Cα*-OMe monomers (**Ufo** and **uo**) result in ∼4°C destabilization for DNA duplexes compared to the unmodified duplex, and a similar trend is observed for DNA:RNA duplexes where ΔT_m = –1.0 to -2.0°C for ON3(**uo**):ON2 and ON3(**Ufo**):ON2, respectively. **Ufme**, containing a 4′-*Cα*-Me, results in even greater destabilization than 4′-*Cα*-OMe substituents by ∼1°C for a given duplex (e.g. compare ON3(**Ufme**):ON4 and ON3(**Ufo**):ON4)). This could be due to a difference in solvation of the more hydrophilic methoxy compared to a methyl group or reduced *N*-type sugar conformation.

Oligonucleotides bearing a chain-inverted 4′-*Cβ*-OMe nucleotide (**Ufob** or **uob**) thermally destabilize duplexes, regardless of the context of the duplex backbone. For example, **Ufob** results in ∼9°C decrease in T_m of RNA (ON1(**Ufob**):ON2) or DNA (ON3(**Ufob**):ON2) duplexes. A similar, but less extreme trend of destabilization is also observed for **uob**, where RNA and DNA homoduplexes display up to 6.3°C decrease in T_m-values. It appears that the 2′-substituent plays a more impactful role in the 4′-*Cβ*-epimers, where 2′-*O*Me (**uob**) is less destabilizing than 2′-F (**Ufob**).

In general, 2′-F- or 2′-*O*Me-4′-*Cα*-modified nucleotides are well tolerated in RNA duplexes, and result in similar T_m-values as the unmodified duplex. Incorporation of these modifications into DNA:RNA or DNA:DNA duplexes results in decreased T_m by up to 5.2°C. However, 2′-F- or 2′-*O*Me-4′-*Cβ*-OMe nucleotides introduce even greater destabilization, particularly in RNA duplexes with up to ∼9°C destabilization with a single incorporation.

Nuclease stability

The stability of these modifications toward 3′-specific exonuclease degradation was evaluated by incubating a series

Table 2. **Ufo**, **Ufme**, **Ufob**, **uo**, **uob** crystal data, data collection and refinement parameters[a]

Structure	Ufme	Ufob	uo	uob	Ufo
Modification	4′-*Cα*-Me,2′-F U	4′-*Cβ*-OMe, 2′-F U	4′-*Cα*-OMe, 2′-*O*Me U	4′-*Cβ*-OMe, 2′-*O*Me U	4′-*Cα*-OMe, 2′-F U (5VR4)
Wavelength [Å]	0.9184	0.918	0.9184	0.9183	0.979
Resolution range [Å]	24.44–1.50 (1.53–1.50)	34.61–2.40 (2.49–2.40)	21.4–1.40 (1.45–1.40)	17.98–1.85 (1.92–1.85)	20.0–1.50 (1.53–1.50)
Space group	$P\,4_3\,2_1\,2$	$P\,2_1\,2_1\,2_1$	$P\,4_3\,2_1\,2$	R 3:H	$P\,4_3\,2_1\,2$
Unit cell *a*, *b*, *c* [Å]	30.46, 30.46, 81.89	47.01, 47.63, 100.74	31.5, 31.5, 85.6	90.44, 90.44, 64.12	44.39, 44.39, 85.92
α, *β*, *γ* [°]	90, 90, 90	90, 90, 90	90, 90, 90	90, 90, 120	90, 90, 90
Total reflections	145,275	117,677	216,602	84,5484	104,936
Unique reflection	6,684 (644)	9,164 (907)	16,014(1,547)	16,493(1,637)	14,409
Multiplicity	21.6 (9.5)	12.8 (12.1)	13.5 (12.3)	51.3 (12.8)	7.3 (7.3)
Completeness [%]	99.6 (99.8)	97.4 (99.0)	98.7 (96.3)	98.4 (98.1)	98.8 (97.6)
<I/σ(I)>	24.5 (2.4)	11.0 (7.5)	11.0 (0.9)	17.9 (1.1)	21.1 (2.7)
Wilson B-factor [Å^2]	14.34	16.54	20.01	35.26	17.95
R-merge	0.101 (0.988)	0.198 (0.433)	0.107 (2.33)	0.144 (2.006)	0.067 (0.795)
R-meas	0.104 (1.04)	0.207 (0.453)	0.111 (2.43)	0.145 (2.093)	0.072 (0.857)
R-pim	0.022 (0.808)	0.058 (0.129)	0.030 (0.684)	0.019 (0.579)	0.027 (0.317)
CC1/2	0.994 (0.808)	0.965 (0.98)	0.997 (0.539)	0.999 (0.478)	(0.943)
Reflections used in refinement	6,672 (664)	9,093 (907)	16 009 (1547)	16 408 (1637)	14 326 (1375)
Reflections used for *R*-free	293 (19)	473 (60)	726 (67)	823 (69)	752 (72)
R-work	0.187 (0.278)	0.206 (0.238)	0.184 (0.277)	0.227 (0.486)	0.186 (0.245)
R-free	0.215 (0.345)	0.243 (0.293)	0.206(0.278)	0.231(0.440)	0.242 (0.321)
Number of non-hydrogen atoms	413	1537	406	1413	814
Macromolecules	349	1360	306	1224	676
Ligands	12	–	36	144	1
solvent	52	177	64	45	137
RMS (bonds) [Å]	0.008	0.006	0.011	0.006	0.009
RMS (angles) [°]	1.2	1.2	1.6	1.1	1.8
Average *B*-factor [Å^2]	21.2	17.1	26.8	45.2	25.6
macromolecules	19.1	16.2	24.4	45.2	23.1
ligands	29.9	–	27.7	46.4	39.9
solvent	33.3	23.7	38.2	40.1	37.6

[a]Numbers in parentheses refer to the outermost shell.

Table 3. Estimated percentages of C3′-*endo* conformers of 4′-modified nucleosides based on ^{1}H-NMR $^3J_{H1'\text{-}H2'}$ coupling constants[a]

	Modification				
Monomer	C2′	C4′	C4″	$J_{1'\text{-}2'}$	%*N*
Uf	F	H	CH_2OH	2.0	∼80
Ufme	F	CH_3	CH_2OH	3.3	∼70
Ufo	F	OCH_3	CH_2OH	<1.0	>90
Ufob	F	CH_2OH	OCH_3	5.6	∼45
u	OCH_3	H	CH_2OH	5.1	∼50[b]
uo	OCH_3	OCH_3	CH_2OH	4.1	∼60
uob	OCH_3	CH_2OH	OCH_3	7.5	∼25
dTo	H	OCH_3	CH_2OH	N/A	∼70[c]

[a]NMR data were obtained in d_6-DMSO. Percentage of *N*-type conformation (%*N*) was calculated by applying the empirical equation $\%N = 100 - 10 \times (J_{H1'}\text{-}J_{H2'})$.
[b]Values from (16).
[c]Values from (35).

of terminally modified oligothymidylate with snake venom phosphodiesterase (SVPD), and monitoring the degradation of the full-length oligonucleotide (Figure 2). A single or double incorporation of 2′-modified nucleotide (ON5(**X**) or ON6(**X**): **X** = **Uf** or **u**) with a canonical phosphodiester backbone is rapidly degraded within 1 h. Addition of a 4′-*Cα*-substituent (**Ufme**, **Ufo** and **uo**) increases the stability, particularly for the double incorporation of **uo** (ON6(**uo**)) with $t_{1/2} = 3.2$ h. Even a single incorporation of 4′-*Cβ*-OMe epimer (**Ufob** or **uob**), regardless of the identity of the 2′-substituent, leads to remarkable stability with >90% of full length oligonucleotide remaining after 24 h (Supplementary Material, Figure S1). This was initially hypothesized to be due to the close proximity (∼4 Å) of the hydrophobic methyl group to the adjacent phosphates, as modeled for **Ufob** (16).

The presence of a phosphorothioate (PS) linkage generally increases the enzymatic stability (Figure 2C,D). Interestingly, in this context, **u** and **uo** display similar re-

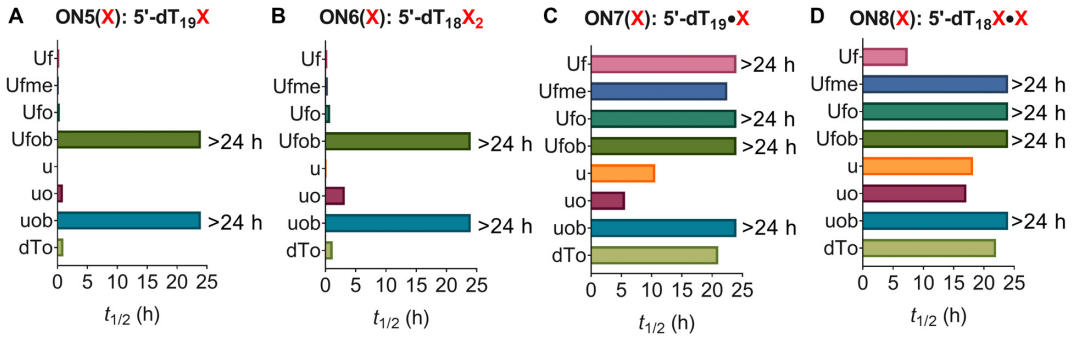

Figure 2. Relative stabilities toward 3′-specific exonuclease degradation. ONs (0.1 mg/ml) with (**A**, **B**) or without (**C**, **D**) additional PS modification (•) were incubated with SVPD (150 mU/ml) in 50 mM Tris (pH 7.2) buffer supplemented with 10 mM $MgCl_2$ and monitored via IEX-HPLC. Decay curves used to calculate half-lives $t_{1/2}$ [h] are shown in Supplementary Figure S1 (Supplementary Materials). Values for **Uf**/**Ufo**/**Ufob** are from ref. 16.

sistance towards degradation of ONs with either a single or double incorporation (compare ON7 and ON8), which suggests the 4′-*C*-substituent might not be the predominant factor governing the observed increased enzymatic stability of 2′-*O*Me/4′-*C*-OMe modified nucleotides. In general, oligonucleotides bearing double incorporations (ON8(**X**)) of the modified nucleotide are more stable towards exonuclease degradation than a single incorporation (ON7(**X**)). Furthermore, it appears that 2′-F/4′-*C*-substituted derivatives are more resistant to degradation than the corresponding 2′-*O*Me derivatives (compare **Ufo**/**Ufme** versus **uo**). However, the 4′-*Cβ* epimers (**Ufob** and **uob**) are remarkably stable towards SVPD degradation. Generally, in the presence of a PS linkage, the order of stability is: **Ufob**/**uob**>>**Ufo**>**Ufme**>**uo**>**Uf**/**u**, where addition of 4′-*C*-substituents to 2′-modified nucleotides results in enhanced enzymatic stability.

Structural effects of 4′-*C*-modifications

To better understand the conformational underpinnings of the stability, nuclease protection and siRNA activities (*vide infra*, Table 4) afforded by the various 4′-*C*-modified nucleotides, we determined crystal structures of RNA octamers C*GAAXUCG (C* = Br5C; **X** = **Ufme**, **Ufob**, **uo**, **uob**). The structure of the corresponding octamer with **Ufo** was reported earlier (16). The five structures were phased by bromine single-wavelength anomalous dispersion (Br-SAD). A summary of crystal data, X-ray diffraction data collection and refinement parameters is given in Table 2. An example of the quality of the final electron density is depicted in Supplementary Figure S2 (Supplementary Material). The crystallographic asymmetric unit (a.u.) contains multiple copies of the modified duplexes in three cases. Thus, the **Ufo** a.u. features two duplexes, and the a.u. for both the **Ufob** and **uob** structures contains four duplexes. The a.u. of **Ufme** and **uo** consists of just a single duplex. We found that individual strands from the same structure exhibit rather similar conformations. Therefore, distances mentioned here represent average values based on two strands (**Ufme**, **uo**), four strands (**Ufo**), or eight strands (**Ufob**, **uob**) unless stated otherwise. Views of 5′-A**X**U-3′ trimers for the **uo**, **Ufme**, **Ufob** and **uob** modifications are depicted in Figure 3.

Table 4. In vitro potency (IC_{50}) of fully modified siRNA targeting *Ttr* mRNA[a]

siRNA	Modification	siRNA sequence	IC_{50} (nM)
1	Parent	*A*•a•*CaGuGuUCUuGcUcUaUaA*Δ u•*U*•a*UaGaGcAagaAcAcUgUu*•u•u	0.08[b]
2	Ufo	*A*•a•*CaGuGuUCUuGcUcUaUaA*Δ u•**Ufo**•a*UaGaGcAagaAcAcUgUu*•u•u	1.32[b]
3	Ufob	*A*•a•*CaGuGuUCUuGcUcUaUaA*Δ u•**Ufob**•a*UaGaGcAagaAcAcUgUu*•u•u	3.78[b]
4	Ufme	*A*•a•*CaGuGuUCUuGcUcUaUaA*Δ u•**Ufme**•a*UaGaGcAagaAcAcUgUu*•u•u	0.28
5	dTo	*A*•a•*CaGuGuUCUuGcUcUaUaA*Δ u•**dTo**•a*UaGaGcAagaAcAcUgUu*•u•u	>10
6	Ufo	*A*•a•*CaGuGuUC***Ufo**u*GcUcUaUaA*Δ u•*U*•a*UaGaGcAagaAcAcUgUu*•u•u	0.06[b]
7	Ufob	*A*•a•*CaGuGuUC***Ufob**u*GcUcUaUaA*Δ u•*U*•a*UaGaGcAagaAcAcUgUu*•u•u	1.83[b]
8	Ufme	*A*•a•*CaGuGuUC***Ufme**u*GcUcUaUaA*Δ u•*U*•a*UaGaGcAagaAcAcUgUu*•u•u	0.1
9	dTo	*A*•a•*CaGuGuUC***dTo**u*GcUcUaUaA*Δ u•*U*•a*UaGaGcAagaAcAcUgUu*•u•u	0.09

[a] siRNA were transfected into primary mouse hepatocytes and target mRNA was quantified after 24 h using real-time PCR. Lowercase = 2′-OMe monomers; italic = 2′-F monomers; • = phosphorothioate (PS) linkage; Δ = triantennary GalNAc ligand (Ref. 8). [b] Ref. 16.

Consistent with the modest effects on the T_m and the lack of significant protection against nuclease degradation afforded in the absence of additional PS modification, the **Ufo** (13), **Ufme** and **uo** backbones exhibit more or less canonical conformations. Thus, the puckers of residues that bracket 4′-*C*-modified uridines and those of modified residues, all fall within the C3′-*endo* range. As well, backbone torsion angles lie in ranges associated with A-form RNA, i.e. *sc*-, *ap*, *sc*+, s*c*+, *ap*, *sc*- (from α to ζ; Figure 3A, B—see Figure 4 in (16) for a depiction of the **Ufo**-modified backbone).

The 4′-*C*-OMe substituent in **uo** and **Ufo** as well as the 4′-*C*-Me group in **Ufme** assume a pseudo-axial orientation and are directed into the minor groove (Figures 3A, B and 4A). The distances between methyl carbon and the 5′- and 3′-adjacent phosphorus atoms range from 4.4 Å (**Ufme**) to 5.8 Å (**uo**). But despite the relatively close spacing between the two moieties, e.g. 4′-*C*-Me and 3′-PO_2 in the case of

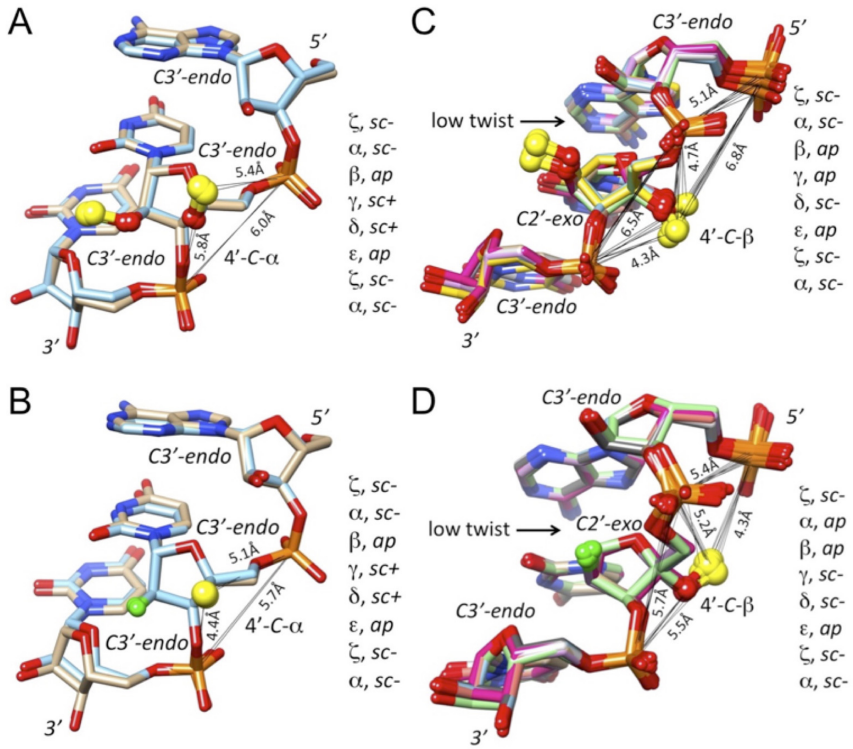

Figure 3. Conformational properties of RNA backbones containing α- or β-epimers of 4′-*C*-modified uridines. Close-up views of the modified residue and 5′- and 3′-adjacent nucleotides: (**A**) **uo**, (**B**) **Ufme**, (**C**) **uob** and (**D**) **Ufob**. Distances are averages based on multiple strands per crystallographic asymmetric unit (A, B: 2; C, D: 8), and backbone torsion angle ranges for modified residues are shown on the right.

Ufme (Figure 3B), the orientation of the 4′-substituents in the α-epimers results only in limited protection against attack by a nuclease. This contrasts with the relative orientations of (*R*)- and (*S*)-5′-*C*-Me substituents and phosphates that also result in a close approach but, in addition, methyl groups being inserted between the 5′- and 3′-adjacent phosphates (15). This structural picture is consistent with 5′-*C*-Me-modified siRNAs dodging nucleases more effectively than those containing 4′-*C*α-modified nucleotides (see the Discussion section).

Unlike the α-epimers, **Ufob** and **Uob** with inverted stereochemistry at C4′ inside RNA locally give rise to drastic deviations from the canonical RNA geometry. The changes include torsion angles (α to δ), sugar pucker (C2′-*exo* for **Ufob** and **uob**), helical twist (nearly absent between **Ufob**/**uob** and the preceding A), very short P-P distances (as tight as 5.1 Å) and a local kink in the backbone (Figures 3C, D, 4). The 4′-substituent is now directed into the major groove and the methyl group is wedged between 5′- and 3′-adjacent phosphates. The structural data thus help rationalize the excellent protection against nuclease attack afforded by the 4′-*C*β-epimers (Figure 2). Tightly spaced phosphates create unfavorable electrostatics (Figure 4BC), and the lack of a twist at the site of modification leads to a tight contact between **Ufob**/**uob** (**X**) sugar and the adjacent adenine base (O4′[**X**]…N9[A] = 3.3 Å; Figure 3CD). These observations can account for the steep loss in stability as a result of **Ufob** or **uob** incorporation into RNA (Table 1).

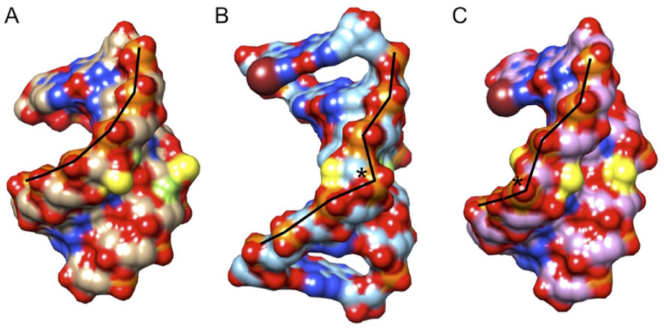

Figure 4. Consequences for RNA backbone conformation of incorporation of 4′-*C*α-OMe and 4′-*C*β-modified uridines. Surface renderings of octamer duplexes containing (**A**) **Ufo**, (**B**) **Ufob** and (**C**) **uob**. The presence of 4′-*C*β-epimers results in a distinct kink in the backbone (marked by an asterisk). Black bars link adjacent phosphorus atoms. Carbon atoms are colored tan (A), light blue (B) and pink (C) and O, N, P and Br atoms are colored red, blue, orange and maroon, respectively. Methyl carbons of 2′-*O*Me and 4′-*C*-OMe substituents are highlighted in yellow and 2′-F atoms are light green.

4′-*C*α-OMe-U and 4′-*C*β-OMe-U Modifications are accepted with the siRNA guide bound to Ago2

In vitro siRNA activity assays were conducted using mouse hepatocytes and targeted mouse transthyretin (*Ttr*) mRNA (Table 4). The reference siRNA for the *Ttr* mRNA activity studies was a 21mer duplex featuring 2′-*O*Me and 2′-F

substituted nucleotides and six PS linkages, combined with a two-nucleotide overhang at the 3′-end of the guide (antisense, AS) strand, and a conjugated GalNAc ligand to facilitate uptake into hepatocytes at the 3′-end of the sense strand (16). Insertion of three **Ufo** residues at positions AS4, AS18 and AS20 had been found earlier to reduce the activity only marginally (IC_{50}: 0.08 and 0.29 nM for native and modified siRNA, respectively) (16). Insertion of **Ufo** at AS2 against *Ttr* mRNA led to significantly reduced activity (IC_{50}: 1.3 nM; Table 4). **Ufob** at the same site lowered the activity even more (IC_{50}: 3.8 nM) and also lowered the activity drastically in the center of the sense siRNA at S11 (IC_{50}: 1.8 nM). Conversely, **Ufme** at AS2 was quite well tolerated (IC_{50}: 0.28 nM) and fared even better at S11, adjacent to the cleavage site (IC_{50}: 0.1 nM; Table 4). In order to better understand possible origins of these site-specific effects on activity by 4′-*C*-modified nucleotides, we turned to the crystal structure of a micro-RNA (AS strand equivalent) bound to human Argonaute 2 (Ago2) (33). We extracted **Ufo** or **Ufob** nucleotides from the crystal structures of modified RNA octamers and fused them with the RNA strand bound to Ago2, essentially leaving the conformations of modified Us untouched. The initial models were energy-minimized using molecular mechanics approaches. The 4′-*C*-OMe methyl group of **Ufo** at AS2 is relatively tightly spaced with the Leu-563 side chain and energy minimization only partially removed the steric conflict (Figure 5A). The 4′-*C*-OMe substituent of **Ufo** at AS4 also faces a hydrophobic region, but can be relatively well accommodated, thus explaining the more modest loss of activity (Figure 5B). For **Ufob** at AS2 a steric conflict arises with the 3′-adjacent G in that the distance between 4′-*C*-OMe methyl carbon and N7 in the model is only ca. 2.8 Å (Figure 5C). In addition, the **Ufob** base does not stack on G3 and its Watson-Crick edge engages in close unfavorable contacts to Thr-559 and Asn-562. We also examined **Ufob** at AS6, a site that is characterized by a distinct kink and closely spaced phosphates (Figure 5D). However, insertion of **Ufob** at that site abolishes stacking with G5, and the uracil base is instead wedged between Q757 and I365, resulting in unfavorable contacts with the latter and A369.

DISCUSSION

We synthesized a series of nucleotide building blocks with combined 2′-(F, *O*Me) and 4′-*C*-modifications (OMe, Me), whereby both the α- and β-epimers were considered at the ribose C4′ position in the case of the methoxy (OMe) substituent. Modified nucleotides were incorporated into oligonucleotides and the effects of individual modifications on the pairing stability, exonuclease resistance and RNAi activity assayed. We determined crystal structures of RNA octamer duplexes, with a single modified uridine nucleotide introduced per strand, in order to gain a better understanding of the origins underlying the consequences of the various 2′,4′-disubstituted nucleotides on RNA stability and activity. The properties of RNA analogs with modifications at the 2′-position have been studied in great detail. For example, in the well-established modification patterns with 2′-F and 2′-*O*Me RNAs, the sugar moieties typically adopt an *N*-type C3′-*endo* pucker that is also preferred by the native ribose (36,37). This sugar conformation places the 2′-substituent in a pseudoaxial orientation that satisfies the gauche effect with O4′.

Adding a second substituent in the form of a 4′-*C*-OMe or -Me group might either perturb the pucker conferred by the 2′-substitution (i.e., 2′-F (**Ufo**, **Ufme**) and 2′-*O*Me RNA (**uo**)) or leave it essentially unchanged. NMR coupling data at the nucleoside level indicate that **Ufo,** just like **Uf** strongly favors the *N*-type pucker (ca. 90% and 80%, respectively). However, the %*N* pucker for **uo** is diminished by comparison (ca. 60%), a degree comparable to those seen for uridine (**u**; ca. 50%) and **dTo** (ca. 70% (35)). The latter nucleoside thus exhibits a tendency to adopt the *N* pucker that matches that of **Ufme**. The crystal structures of octamers with incorporated **Ufo** (16), **uo** (Figure 3A) and **Ufme** (Figure 3B) residues demonstrate that all modified sugars adopt the C3′-*endo* pucker, consistent with the preference established at the nucleoside level. Therefore, both substituents assume a pseudoaxial orientation and in the case of the 4′-*Cα*-OMe and -Me groups, that is consistent with the anomeric effect. For the β-epimers i.e., **Ufob** and **uob**, the NMR data are consistent with a much-diminished tendency for an *N*-type pucker at the nucleoside level. However, in the crystal structures of modified octamers all 4′-*Cβ*-modified uridines exhibit a C2′-*exo N*-type sugar conformation (Figure 3C,D), a 36° sector in the pseudorotation phase angle cycle that is adjacent to C3′-*endo*.

Incorporation of the 4′-*Cα* epimer **Ufme**, **Ufo** and **uo** has a neutral effect on the stability of a modified RNA:RNA duplex, but the analogs exert a destabilizing influence when incorporated into the RNA strand of RNA:DNA hybrids or within DNA:DNA duplexes. Given their preference for an RNA-like sugar conformation, this is not surprising. Still, the 4′-*Cα*-substituent does not promote an increased stability beyond the positive effect afforded by the 2′-substitution alone. In fact, **Uf** alone results in a T_m increase of around 1°C per modification, and if anything, the combination with the 4′-modification appears to neutralize that gain. Multiple reasons could account for the slight loss in stability, among them the relatively close spacing of the 2′- and 4′-substituents and the insertion of a hydrophobic moiety between phosphates. It is interesting to note that **dTo** stabilizes an RNA duplex by ∼2°C per modification (Table 1). Pinpointing the origin(s) of the slight loss in stability seen with **Ufo**, **Ufme** and **uo** relative to **Uf** may be quite challenging. Finally, the recently evaluated 4′-*Cα*-aminoalkyl-2′-*O*-methyl modifications appear to be more destabilizing in the context of RNA duplexes than the 4′-*Cα*-OMe and 4′-*Cα*-Me substituted uridines examined here as the former resulted in T_m losses of between –2.0 and –2.3°C per incorporated nucleotide (38).

By comparison, it is not surprising that the 4′-*Cβ* epimers **Ufob** and **uob** are strongly destabilizing. The crystal structures of modified octamers reveal tight phosphate-phosphate and 4′-*Cβ*-OMe-phosphate spacings consistent with unfavorable electrostatic and steric effects (Figure 3C,D). It is noteworthy that **Ufob** is significantly more destabilizing than **uob** (−8.9°C and –6.3°C, respectively, Table 1). Close inspection of the structures shows that the average P-P and Me-P distances at the site of the modifica-

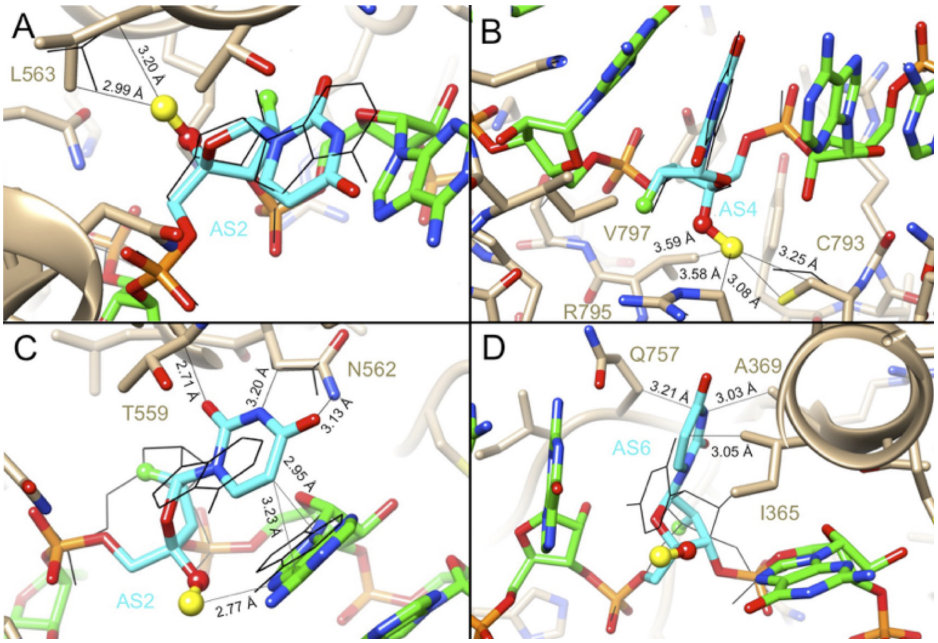

Figure 5. Modelled interactions between 2′-F/4′-*C*-OMe-Us in antisense (AS) siRNA and human Ago2. (**A**) **Ufo** at position 2 (AS2), (**B**) **Ufo** at AS4, (**C**) **Ufob** at AS2 and (**D**) **Ufob** at AS6. Models are based on the crystal structure of the complex between Ago2 and miRNA-20a that contains A at positions 2 and 4, and **U** at position 6 (33). Carbon atoms of modified Us are highlighted in cyan, and 2′-fluorine (light green) as well as 4′-*C*-substituent atoms (oxygen, red, and methyl carbon, yellow) are drawn as spheres. Orientations of corresponding residues in the native complex are shown in wire mode and distances between selected atoms of modified Us and amino acids in the refined model are shown as thin lines with distances in Å.

tion are somewhat tighter for **Ufob** than **uob**, thus providing a rationalization of the observed difference in the melting temperature. Another interesting difference between the **Ufob** and **uob** modifications is the inverted spacing between methyl groups from the 4′-*C*-substituent and the N – 1 and N + 1 phosphates, 3′- and 5′-adjacent nucleotides, (N being the modified nucleotide) in the two structures. Thus, in the **uob**-modified octamer, the methyl group is positioned closer to the N + 1 phosphate (average 4.3 Å versus 6.8 Å to N – 1; Figure 3C), whereas in the **Ufob**-modified octamer, the methyl group sits nearer to the N – 1 phosphate (4.3 Å versus 5.5 Å to N + 1; Figure 3D).

It is perhaps surprising that **Ufob** and **uob** exhibit stacking and Watson-Crick base pairing despite the inverted stereochemistry at C4′. However, in addition to the kinked backbone at the modification sites in **Ufob** and **uob** containing duplexes (Figure 4), the two structures also display a virtual absence of a helical twist between modified uridines and the preceding A nucleotide. This results in O4′ from **Ufob** and **uob** being positioned directly under the five-membered ring of adenine (sugar-base stacking; Figure 6). The twist between modified residues and the 3′-adjacent uridine is within the expected range for an A-form RNA.

We recently conducted an investigation of the influence of glycol nucleic acid (GNA) residues inside RNA on structure and siRNA activity, and observed chirality-dependent enhancements of potency (39). (*S*)-GNA is well tolerated in an RNA strand but does result in non-canonical separation of phosphates at incorporation sites owing to the shorter backbone of GNA relative to RNA. (*R*)-GNA causes larger drops in T_m values than (*S*)-GNA and kinks the backbone locally. (*S*)-GNA inserted at position 6 of the guide strand

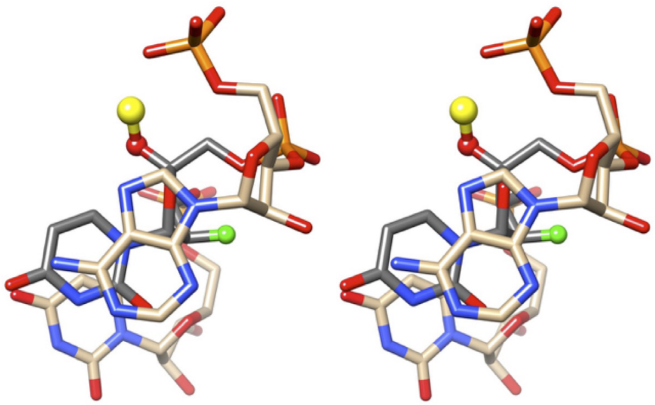

Figure 6. Cross-eye stereo illustration depicting the pA5**pUfob6**pU7 trimer viewed approximately along the normal to the adenine plane. The glycosidic bonds of A5 and **Ufob6** are nearly parallel, indicating the virtual absence of a helical twist at that base step. Carbon atoms of the modified uridine are colored in gray and 4′-*C*-OMe carbon and 2′-F are highlighted as solid spheres colored in yellow and green, respectively.

triggered higher activity relative to parent siRNA, and appeared well suited at a location where adjacent phosphates are more closely spaced as a result of a distinct kink (Figure 5D). However, (*R*)-GNA was not tolerated at the same site, despite its penchant for perturbing the backbone. This is somewhat reminiscent of the conformational consequences of **Ufob** and **uob** that do not appear to be a good match for the site of the kink in guide siRNA between residues 6 and 7 (Figure 5D). Their non-canonical conformational features seem to be too extreme to be tolerated even at this site, which is severely kinked by Ago2.

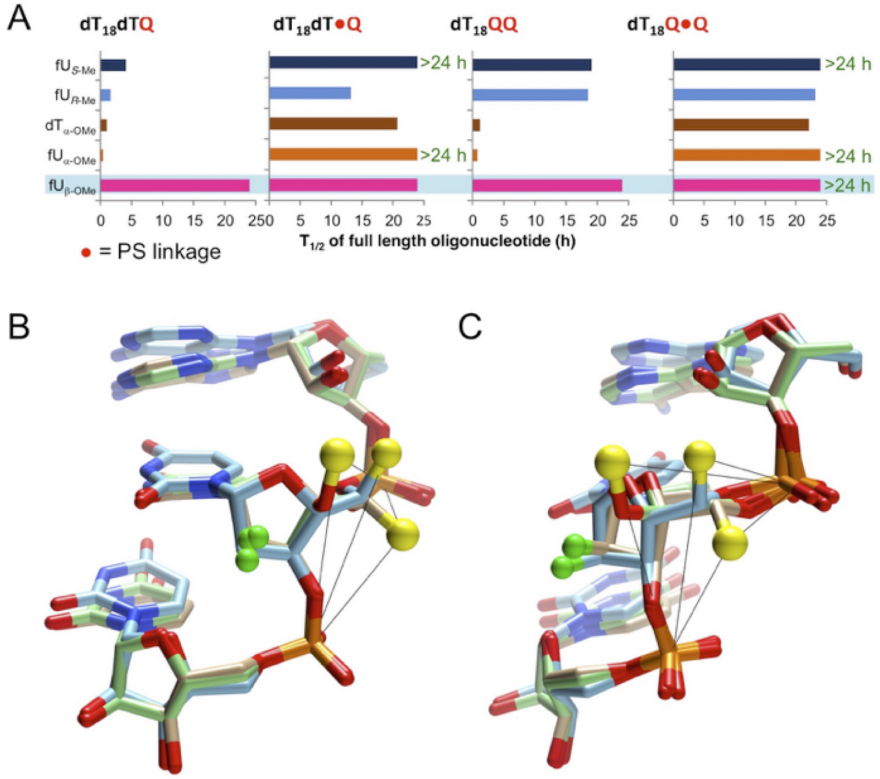

Figure 7. Relative protection against exonuclease degradation (SVPD) afforded by the 5′-*C*-Me (15) and 4′-*Cα*-OMe (**Ufo**) modifications. (**A**) Outcome of nuclease assays comparing oligo-2′- deoxynucleotides with 3′-terminal 2′-F,5′-*C*-Me-U ($fU_{S\text{-}Me}$ is (*S*)-5′-*C*-Me and $fU_{R\text{-}Me}$ is (*R*)-5′-*C*-Me) or **Ufo** modifications with or without PS linkages. Overlay of trimers with a central modified uridine viewed (**B**) from the minor groove and (**C**) across the minor and major grooves. Color code: A[(*S*)-5′-*C*-Me-U]U, light blue carbons; A[(*R*)-5′-*C*-Me-U]U, tan carbons; A[**Ufo**]U, green carbons. 4′-*C*-OMe and 5′-*C*-Me carbons are shown as yellow spheres and 2′-F are shown as green spheres. The structural overlay demonstrates the different orientations of the 4′-*C*- and 5′-*C*-substituents relative to the 5′- and 3′-adjacent phosphate groups. Thus, 5′-*C*-methyl groups are positioned in closer proximity to phosphates, and the (*R*)-5′-*C*-Me group is effectively wedged between them. Structural data for 5′-*C*-modified backbones were taken from (15).

Ufo inserted into the guide and passenger strands at several locations including AS4 reduced the activity only marginally (Table 4) (16), consistent with the absence of obvious unfavorable contacts in models of the complex between siRNA and Ago2 (e.g. AS4, Figure 5B). At AS2 **Ufo** triggers reduced activity by comparison (Figure 5A), but still fares considerably better than **Ufob** (Figure 5C). Based on our molecular modeling study, it is clear that **Ufme** would a better fit at AS2 than **Ufo**, consistent with the in vitro activity data (Table 4). Thus, we expect the smaller 4′-*C*-Me substituent of **Ufme** to be more easily accommodated opposite L563 (Figure 5A). It is noteworthy that among the 2′-substituents tested at AS2, only fluorine is tolerated (2′-*O*Me is not) (Figure 5A). Thus, the most advanced siRNA drug candidate patisiran features 2′-ribose residues at the AS1 and AS2 positions, at the 5′-end of the guide siRNA (1).

The local conformational distortion of the backbone caused by **Ufob** and **uob** as well as the tight spacing between the 4′-*C*-methoxy group and phosphates likely facilitate the strong protection against exonuclease degradation afforded by these modifications relative to **Ufo**, **Ufme** and **uo**. **Ufo** and **Ufme** are more effective at stabilizing against SVPD than **uo**, particularly in combination with the PS modification (Figure 2). Indeed, **Ufme** shows Me-P contacts that are tighter than those seen in **Ufo** and **uo** (Figure 3). Moreover, those distances are slightly shorter in **Ufo** than in **uo**. But perhaps the 2′-substituent is more important in regard to nuclease protection in these two latter modifications than the 4′-*C*-substituent. Specifically, fluorine might keep the ribose more rigid than the methoxy group and therefore prevent the exonuclease from avoiding close contacts with the 4′-*C*-OMe substituent. Close contacts between a backbone substituent and the 5′- and 3′-adjacent phosphate groups are key indicators of robust protection against nucleolytic attack and this is also demonstrated by our previous studies of RNAs with (*R*)-5′-*C*-Me and (*S*)-5′-*C*-Me modifications (15). Nuclease degradation assays using SVPD demonstrated that the 5′-modified analogs afford better protection than **Ufo**, particularly in the absence of additional PS modification (Figure 7A). Crystal structures of modified duplexes provide a rationalization for this finding in that the methyl group of the 5′-*C*-modified backbones is positioned closer to the phosphates on average than 4′-*C*-OMe (Figure 7B, C).

In summary, crystallographic data for RNAs with **Ufo**, **Ufob**, **Ufme**, **uo** or **uob** residues provide insight into the stability, nuclease resistance and activity of siRNAs containing 4′-*C*-modified residues. Notes added in proof: Prior to acceptance of the revised version of this manuscript, a pa-

per reporting the synthesis of **uo** and its incorporation into siRNAs appeared on-line (40).

DATA AVAILABILITY

Coordinates and structure factors for the five duplexes have been deposited in the Protein Data Bank (http://www.rcsb.org) with PDB ID accession numbers: 5VR4, Ufo; 6CXZ, Ufme; 6CY0, Ufob; 6CY2, uo; 6CY4, uob.

SUPPLEMENTARY DATA

Supplementary Data are available at NAR Online.

ACKNOWLEDGEMENTS

This research used resources of the Advanced Photon Source, a U.S. Department of Energy (DOE) Office of Science User Facility operated for the DOE Office of Science by Argonne National Laboratory under Contract No. DE-AC02-06CH11357. Use of the LS-CAT Sector 21 was supported by the Michigan Economic Development Corporation and the Michigan Technology Tri-Corridor (Grant 085P1000817).

FUNDING

Alnylam Pharmaceuticals, Vanderbilt University; U.S. NIH [R01 GM074161]. Funding for open access charge: Alnylam Pharmaceuticals.

Conflict of interest statement. D.C.G., A.B., S.M., N.T., I.Z., K.C., M.M., K.G.R. and M.M. are employees of Alnylam Pharmaceuticals.

REFERENCES

1. Shen,X. and Corey,D.R. (2018) Chemistry, mechanism and clinical status of antisense oligonucleotides and duplex RNAs. *Nucleic Acids Res.*, **46**, 1584–1600.
2. Hagmann,W.K. (2008) The many roles for fluorine in medicinal chemistry. *J. Med. Chem.*, **51**, 4359–4369.
3. Guo,F., Qiang Li,Q. and Zhou,C. (2017) Synthesis and biological applications of fluoro-modified nucleic acids. *Org. Biomol. Chem.*, **15**, 9552–9565.
4. Merki,E., Graham,M.J., Mullick,A.E., Miller,E.R., Crooke,R.M., Pitas,R.E., Witztum,J.L. and Tsimikas,S. (2008) Antisense oligonucleotide directed to human apolipoprotein B-100 reduces lipoprotein(a) levels and oxidized phospholipids on human apolipoprotein B-100 particles in lipoprotein(a) transgenic mice. *Circulation*, **118**, 743–753.
5. El Harchaoui,K., Akdim,F., Stroes,E.S., Trip,M.D. and Kastelein,J.J. (2008) Current and future pharmacologic options for the management of patients unable to achieve low-density lipoprotein-cholesterol goals with statins. *Am. J Cardiovasc. Drugs*, **8**, 233–242.
6. Finkel,R.S, Chiriboga,C.A., Vajsar,J., Day,J.W., Montes,J., De Vivo,D.C., Yamashita,M., Rigo,F., Hung,G., Schneider,E. *et al.* (2016) Treatment of infantile-onset spinal muscular atrophy with nusinersen: a phase 2, open-label, dose-escalation study. *Lancet*, **388**, 3017–3026.
7. Crooke,S.T., Witztum,J.L., Bennett,C.F. and Baker,B.F. (2018) RNA-targeted therapeutics. *Cell Metab.*, **27**, 714–739.
8. Nair,J.K., Willoughby,J.L., Chan,A., Charisse,K., Alam,M.R., Wang,Q., Hoekstra,M., Kandasamy,P., Kel'in,A.V., Milstein,S. *et al.* (2014) Multivalent N-acetylgalactosamine-conjugated siRNA localizes in hepatocytes and elicits robust RNAi-mediated gene silencing. *J. Am. Chem. Soc.*, **136**, 16958–16961.
9. Matsuda,S., Keiser,K., Nair,J.K., Charisse,K., Manoharan,R.M., Kretschmer,P., Peng,C.G., V Kel'in,A., Kandasamy,P., Willoughby,J.L.S. *et al.* (2015) siRNA conjugates carrying sequentially assembled trivalent *N*-acetylgalactosamine linked through nucleosides elicit robust gene silencing in vivo in hepatocytes. *ACS Chem. Biol.*, **10**, 1181–1187.
10. Rajeev,K.G., Nair,J.K., Jayaraman,M., Charisse,K., Taneja,N., O'Shea,J., Willoughby,J.L.S., Yucius,K., Nguyen,T., Shulga-Morskaya,S. *et al.* (2015) Hepatocyte-specific delivery of siRNAs conjugated to novel non-nucleosidic trivalent *N*-acetylgalactosamine elicits robust gene silencing in vivo. *ChemBioChem*, **16**, 903–908.
11. Nair,J.K., Attarwala,H., Sehgal,A., Wang,Q., Aluri,K., Zhang,X., Gao,M., Liu,J., Indrakanti,R., Schofield,S. *et al.* (2017) Impact of enhanced metabolic stability on pharmacokinetics and pharmacodynamics of GalNAc–siRNA conjugates. *Nucleic Acids Res.*, **45**, 10969–10977.
12. Willoughby,J.L.S., Chan,A., Sehgal,A., Butler,J.S., Nair,J.K., Racie,T., Shulga-Morskaya,S., Nguyen,T., Qian,K., Yucius,K. *et al.* (2018) Evaluation of GalNAc–siRNA conjugate activity in pre-clinical animal models with reduced asialoglycoprotein receptor expression. *Mol. Ther.*, **26**, 105–114.
13. Foster,D.J., Brown,C.R., Shaikh,S., Trapp,C., Schlegel,M.K., Qian,K., Sehgal,A., Rajeev,K.G., Jadhav,V., Manoharan,M. *et al.* (2018) Advanced siRNA designs further improve in vivo performance of GalNAc–siRNA conjugates. *Mol. Ther.*, **26**, 708–717.
14. Janas,M.M., Schlegel,M.K., Harbison,C.E., Yilmaz,V.O., Jiang,Y., Parmar,R., Zlatev,I., Castoreno,A., Xu,H., Shulga-Morskaya,S. *et al.* (2018) Selection of GalNAc-conjugated siRNAs with limited off-target-driven rat hepatotoxicity. *Nat. Commun.*, **9**, 723.
15. Kel'in,A., Zlatev,I., Harp,J., Jayaraman,M., Bisbe,A., O'Shea,J., Taneja,N., Manoharan,R.M., Khan,S., Charisse,K. *et al.* (2016) Structural basis of duplex thermodynamic stability and enhanced nuclease resistance of 5′-methyl pyrimidine-modified oligonucleotides. *J. Org. Chem.*, **81**, 2261–2279.
16. Malek-Adamian,E., Guenther,D., Matsuda,S., Martinez-Montero,S., Zlatev,I., Harp,J., Burai Patrascu,M., Foster,D.J., Fakhoury,J., Perkins,L. *et al.* (2017) 4′-*C*-Methoxy-2′-deoxy-2′-fluoro modified ribonucleotides improve metabolic stability and elicit efficient RNAi-mediated gene silencing. *J. Am. Chem. Soc.*, **139**, 14542–14555.
17. Liboska,R., Snášel,J., Barvík,I., Buděšínský,M., Pohl,R., Točík,Z., Páv,O., Rejman,D., Novák,P. and Rosenberg,I. (2011) 4′-Alkoxy oligodeoxynucleotides: a novel class of RNA mimics. *Org. Biomol. Chem.*, **9**, 8261–8267.
18. Petrová,M., Páv,O., Buděšínský,M., Zborníková,E., Novák,P., Rosenbergová,Š., Pačes,O., Liboska,R., Dvořáková,I., Šimák,O. *et al.* (2015) Straightforward synthesis of purine 4′-alkoxy-2′-deoxynucleosides: first report of mixed purine-pyrimidine 4′-alkoxyoligodeoxynucleotides as new RNA mimics. *Org. Lett.*, **17**, 3426–3429.
19. Martínez-Montero,S., Deleavey,G.F., Kulkarni,A., Martín-Pintado,N., Lindovska,P., Thomson,M., Gonzaález,C., Götte,M. and Damha,M.J. (2014) Rigid 2′,4′-difluororibonucleosides: synthesis, conformational analysis, and incorporation into nascent RNA by HCV polymerase. *J. Org. Chem.*, **79**, 5627–5635.
20. Martínez-Montero,S., Deleavey,G.F., Dierker-Viik,A., Lindovska,P., Ilina,T., Portella,G., Orozco,M., Parniak,M.A., González,C. and Damha,M.J. (2015) Synthesis and properties of 2′-deoxy-2′,4′-difluoroarabinose-modified nucleic acids. *J. Org. Chem.*, **80**, 3083–3091.
21. Martínez-Montero,S., Deleavey,G.F., Martín-Pintado,N., Fakhoury,J.F., González,C. and Damha,M.J. (2015) Locked 2′-deoxy-2′,4′-difluororibo modified nucleic acids: thermal stability, structural studies, and siRNA activity. *ACS Chem. Biol.*, **10**, 2016–2023.
22. Parmar,R., Brown,C., Matsuda,S., Willoughby,J., Theile,C., Charisse,K., Foster,D.J., Zlatev,I., Jadhav,V., Maier,M. *et al.* (2018) Facile synthesis, geometry and 2′-substituent-dependent in vivo activity of 5′-(*E*)- and 5′-(*Z*)-vinylphosphonate-modified siRNA conjugates. *J. Med. Chem.*, **61**, 734–744.
23. Beigelman,L., Deval,J. and Jin,Z. (2017) Substituted nucleosides, nucleotides and analogs thereof. United States Patent No. 9,815,864 B2.

24. Winter,G. (2010) *xia2*: an expert system for macromolecular crystallography data reduction. *J. Appl. Crystallogr.*, **43**, 186–190.
25. Waterman,D.G., Winter,G., Parkhurst,J.M., Fuentes-Montero,L., Hattne,J., Brewster,A., Sauter,N.K. and Evans,G. (2013) The DIALS framework for integration software. *CCP4 Newsletter on Protein Crystallography*, 16–19.
26. Sheldrick,G.M. *SHELXC*. Goettingen University.
27. Schneider,T.R. (2002) Sheldrick, G.M. Substructure solution with SHELXD. *Acta Cryst. Sect. D, Biol. Crystallogr.*, **58**, 1772–1779.
28. Sheldrick,G.M. (2002) Macromolecular phasing with SHELXE. *Z. Kristallogr.*, **217**, 644–650.
29. Pape,T. and Schneider,T.R. (2004) HKL2MAP: a graphical user interface for phasing with SHELX programs. *J. Appl. Crystallogr.*, **37**, 843–844.
30. Emsley,P., Lohkamp,B., Scott,W.G. and Cowtan,K. (2010) Features and development of Coot. *Acta Cryst. Sect. D, Biol. Crystallogr.*, **66**, 486–501.
31. Schuüttelkopf,A.W. and van Aalten,D.M.F. (2004) PRODRG: a tool for high-throughput crystallography of protein-ligand complexes. *Acta Cryst. Sect., Biol. Crystallog.*, **60**, 1355–1363.
32. Adams,P.D., Afonine,P.V., Bunkoczi,G., Chen,V.B., Davis,I.W., Echols,N., Headd,J.J., Hung,L.-W., Kapral,G.J., Grosse-Kunstleve,R.W. *et al.* (2010) PHENIX: a comprehensive Python based system for macromolecular structure solution. *Acta Cryst. Sect. D, Biol. Crystallogr.*, **66**, 213–221.
33. Elkayam,E., Kuhn,C.D., Tocilj,A., Haase,A.D., Greene,E.M., Hannon,G.J. and Joshua-Tor,L. (2012) The structure of human argonaute-2 in complex with miR-20a. *Cell*, **150**, 100–110.
34. Pettersen,E.F., Goddard,T.D., Huang,C.C., Couch,G.S., Greenblatt,D.M., Meng,E.C. and Ferrin,T.E. (2004) UCSF Chimera—a visualization system for exploratory research and analysis. *J. Comp. Chem.*, **25**, 1605–1612.
35. Tong,W., Agback,P. and Chattopadhyaya,J. (1993) Synthesis of diastereomerically pure 4′-alkoxy-α (L)- & β (D)-nucleosides and their conformational analysis by 500 MHz ^{1}H-NMR spectroscopy. *Acta Chem. Scand.*, **47**, 145–156.
36. Pallan,P.S., Greene,E., Jicman,P., Pandey,R., Manoharan,M., Rozners,E. and Egli,M. (2011) Unexpected origins of the enhanced pairing affinity of 2′-fluoro-modified RNA. *Nucleic Acids Res.*, **39**, 3482–3495.
37. Lubini,P., Zürcher,W. and Egli,M. (1994) Crystal structure of an oligodeoxynucleotide duplex containing 2′-*O*-methylated adenosines. *Chem. Biol.*, **1**, 39–45.
38. Koizumia,K., Maedaa,Y., Kanoa,T., Yoshidae,H., Sakamotod,T., Yamagishie,K. and Ueno,Y. (2018) Synthesis of 4′-*C*-aminoalkyl-2′-*O*-methyl modified RNA and their biological properties. *Bioorg. Med. Chem.*, **26**, 3521–3534.
39. Schlegel,M.K., Foster,D.J., Kel'in,A., Zlatev,I., Bisbe,A., Jayaraman,M., Lackey,J., Rajeev,K., Charisse,K., Harp,J. *et al.* (2017) Chirality dependent potency enhancement and structural impact of glycol nucleic acid modification on siRNA. *J. Am. Chem. Soc.*, **139**, 8537–8546.
40. Malek-Adamian,E., Patrascu,M.B., Jana,S.K., Martinez-Montero,S., Moitessier,N. and Damha,M.J. (2018) Adjusting the structure of 2′-modified nucleosides and oligonucleotides via C4′-α-F or C4′-α-OMe substitution: synthesis and conformational analysis. *J. Org. Chem.*, doi:10.1021/acs.joc.8b01329.